Center for Alternative Fuels, Engines & Emissions
West Virginia University

Heavy-Duty Vehicle Diesel Engine Efficiency Evaluation and Energy Audit

October 2014

Final Report

Arvind Thiruvengadam, Ph.D. – Principal Investigator
Saroj Pradhan
Pragalath Thiruvengadam
Marc Besch
Daniel Carder
Mechanical and Aerospace Department
West Virginia University,
Morgantown, WV

Oscar Delgado, Ph.D.
The International Council on Clean Transportation
Washington, DC

Table of Contents

ACKNOWLEDGEMENTS

The West Virginia University Center for Alternative Fuels, Engines and Emissions would like to thank the International Council for Clean Transportation (ICCT) for funding this study. We thank Volvo Technology North America for supporting test cell integration of their engine, and thank Cummins Inc. for donating a medium-duty diesel engine for research purposes. In addition, we thank the Cummins and Volvo teams, Dr. Rachel Muncrief, and Fanta Kamakaté, for their reviews and input on an earlier version of the report. We also thank Dr. Oscar Delgado for being the technical lead from the ICCT and Dr. Nic Lutsey for providing valuable inputs during the course of the study.

EXECUTIVE SUMMARY

The modern diesel engine, the primary propulsion source for most heavy-duty vehicle freight movement, is subject to many design constraints, including durability, efficiency, and low emissions. The most stringent emission regulations, for example those in the United States and Europe, require greatly reduced oxides of nitrogen and particulate matter emissions. Heavy-duty vehicle fleet operators and freight shippers demand increased engine efficiency and reliability. Increasingly, new efficiency and greenhouse gas (GHG) emission standards are requiring further improvements in engine efficiency.

This work sought to further understand the engine efficiency, energy losses, and prospects for improvement in diesel engines for heavy-duty vehicles. The project's approach involved laboratory engine testing and analysis of heavy-duty and medium-duty diesel engines that are compliant with the 2010 U.S. Environmental Protection Agency (US EPA) emissions standards. The two primary reference engines tested were a model year 2011 12.8-liter heavy-duty diesel engine, a representative engine for Class 8 tractor-trailers, and a model year 2013 6.7-liter medium-duty engine, representative of Class 4-6 trucks (e.g., urban delivery, vocational). In addition, data from industry colleagues and from the research literature were utilized to understand the change in energy flows and losses due to various efficiency technologies.

The two primary outputs from this study were the characterization of the engines' fuel consumption maps, and detailed energy audit analyses across varying engine speed-load conditions. The engine mapping of fuel consumption included laboratory testing on a 40 CFR 1065 compliant engine dynamometer laboratory at West Virginia University's Center for Alternative Fuels, Engines and Emissions (CAFEE). The process to develop the engine maps included test cycles created using design of experiments (DOE) and curve fitting approach to ascertain a wide range of fueling events that cannot be captured by traditional steady-state test cycles such as the Supplemental Emission Test (SET) and European Stationary Cycle (ESC). The energy audits utilized data that included in-cylinder pressure measurements to estimate indicated work, flow rate and temperature measurements at various locations of the engine to estimate energy flows, and motoring and individual component testing to estimate friction and pumping losses.

The reference heavy-duty diesel engine converted 39.1% of its fuel energy to brake power over the SET engine cycle, with 35.5% lost as exhaust heat, 10.6% lost to engine coolant heat transfer, 6% lost through heat rejected from the charge air cooler (CAC), 3.4% lost as heat to the surrounding ambient air, 2.3% lost to friction of engine components, 1.7% lost to engine pumping, and 1.3% consumed by parasitic losses due to engine accessories such as water and oil pumps. The contribution of EGR cooling to the engine coolant circuit is of the order of 46% of the total heat carried by the coolant. While the reference medium-duty diesel engine over the FTP cycle converted 29.2% of its fuel energy to brake power, 31.4% of fuel energy was lost through exhaust gases, 18.4% of energy loss is attributed to friction and pumping loss, 10% of fuel energy was rejected through the coolant circuit, CAC rejected 5% of fuel energy, 3.6% of fuel energy is attributed to heat transfer to ambient air, and 2.4% of fuel energy was consumed by engine accessories.

The assessment investigated emerging technologies that have the ability to reduce fuel consumption by targeting different energy loss mechanisms. Two potential future engines were analyzed: (1) a "2017 engine" for compliance with heavy-duty vehicle GHG engine standards, and (2) a "2020+ engine" that utilizes more advanced technologies for further fuel consumption reduction from the reference diesel engine. The investigation of emerging technologies to achieve the increased efficiency includes improvements to combustion from increased compression ratio and peak in-cylinder pressures. In

addition, reduction in pumping losses through low-pressure drop aftertreatment systems, low pressure drop EGR loops, reduced EGR and improved turbocharging technology were considered. The reduction in frictional parasitic losses was attributed to the development of advanced lubricants, engine material coatings that lower friction, variable speed water pump and oil pump. Finally, a simulation of an Organic Rankine Cycle (ORC) waste heat recovery (WHR) system was performed to assess its contribution towards engine efficiency improvements.

The simulation focused on using a thermodynamic approach to project fuel consumption of future engine technologies by reducing individual loss categories by a certain magnitude as identified by technology pathways through previous research. Estimated 2017 fuel consumption maps were developed to represent engine fuel consumption that would achieve compliance with the US EPA greenhouse gas standard (GHG) for heavy- and medium-duty engines. Figure 1 illustrates the total energy consumed over the regulatory SET cycle for the reference 2010, estimated 2017, and 2020 and later engines. The estimated 2017 engine technology achieved an average 7.9% fuel consumption reduction over the SET engine cycle, while the more advanced 2020+ engine achieved an average 18.3% fuel consumption reduction in comparison to baseline 2010 heavy-duty engine. The peak BTE of the 2020+ engine was projected to be 49%, and the waste heat recovery simulation improved the BTE of the 2020+ engine to 52%. The reductions were based on a baseline 2010 engine, with a brake-specific CO_2 of 498 g/bhp-hr over the SET. The baseline brake specific-CO_2 emissions is an approximation based on the mass of fuel consumed and not a result of emissions measurement. The fuel consumption reduction for the 2017 engine was factored to achieve at a minimum the 2017 CO_2 standard of 460 g/bhp-hr.

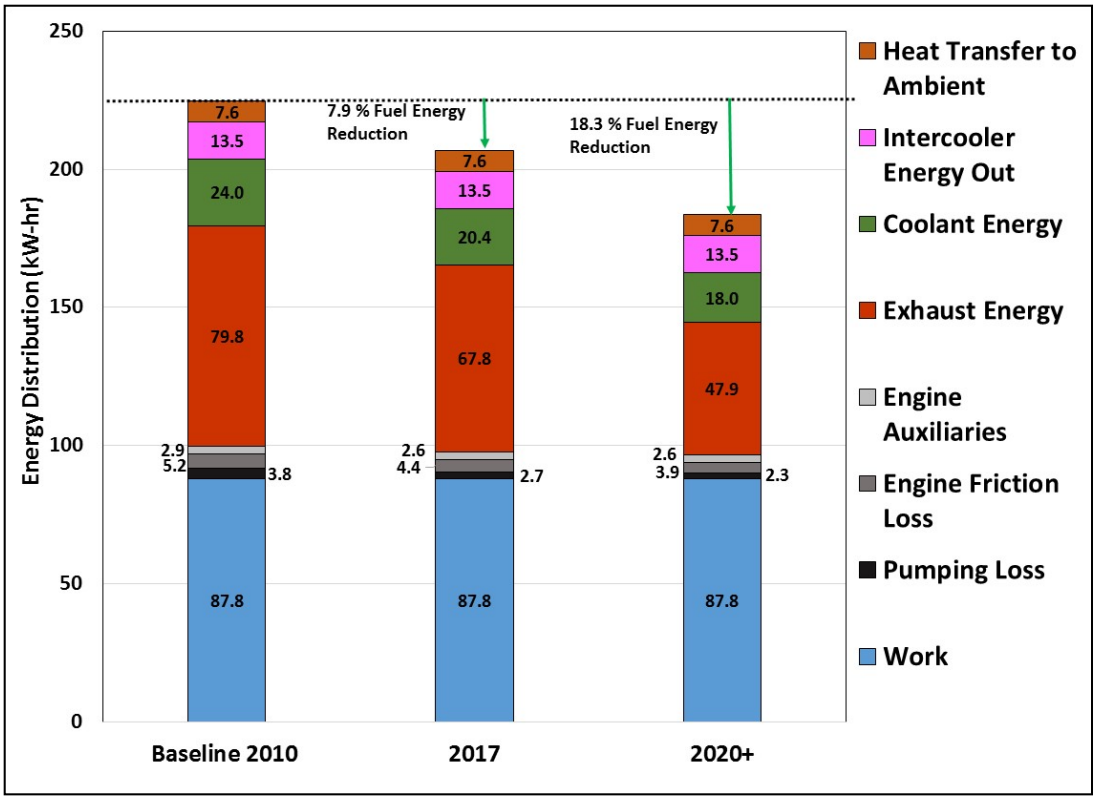

Figure 1 Energy audit results for reference heavy-duty engine, and estimated 2017 and 2020+ engine technologies over the SET cycle

The energy distribution of a reference 2013 medium-duty engine and the estimation of its energy distribution for 2017 and 2020+ engine technologies over the FTP are shown in Figure 2. The 2017 medium-duty technology resulted in 10.6% reduction in estimated fuel consumption compared to the reference 2013 engine to achieve at a minimum 2017 US EPA standard of 576 g/bhp-hr CO_2. The fuel consumption reduction for the advanced 2020+ medium-duty engine was projected to be 19.5%.

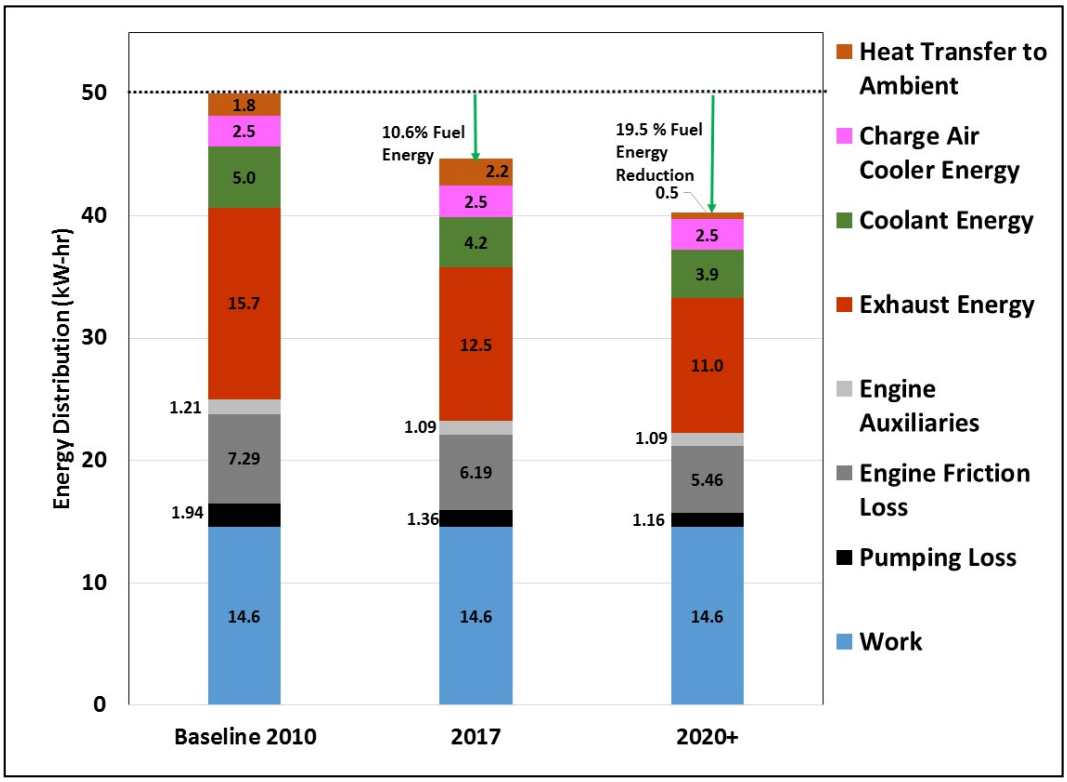

Figure 2 Energy audit results for reference medium-duty engine, and estimated 2017 and 2020+ engine technologies for the FTP cycle

The assessment of potential future engine characteristics presented in this study considers a best-case scenario of chosen technology advancements. The study presents a holistic view of the possible benefits that could be achieved by improving certain loss mechanisms. An objective of the fuel consumption analysis performed in this study was to develop a 2017 engine fuel map that would be compliant with the SET 460 gCO_2/bhp-hr heavy-duty and with the FTP 576 gCO_2/bhp-hr medium heavy-duty GHG standards for 2017 and beyond. The distribution of energy among the various loss categories in real-world future engines could be different from the projections shown in this study, since the energy distribution of future engines will be dependent on the actual pathways and technology approaches adopted by the various manufacturers.

This research makes novel contributions in providing a detailed breakdown of engine energy loads and losses for a modern diesel engine, as well as estimates of technical efficiency potential for future engines. The research points to many areas where future research will better inform the potential for heavy-duty diesel efficiency improvements. For example, integrating an energy flow study of this kind with full-vehicle simulation will be critical to understanding the engine-transmission and powertrain-vehicle load interactions with emerging efficiency technologies for the 2020-2030 timeframe.

1 INTRODUCTION

The heavy-duty diesel engine, the primary propulsion source for most heavy-duty vehicle freight movement, is subject to many design constraints, including durability, efficiency, and low emissions. There is a need for increased engine efficiency and reliability by heavy-duty vehicle fleet operators and freight shippers. More stringent fuel consumption and greenhouse gas (GHG) emission standards are requiring further improvements in engine efficiency.

The transportation sector is one of the largest consumers of petroleum in the U.S. Heavy-duty vehicle diesel consumption is projected to increase for the next several decades, while the largest energy user in the transportation sector, automobiles, is projected to have declining fuel use (EIA, 2013).

With recent presidential directives to improve energy security, Environmental Protection Agency (EPA) and National Highway Traffic Safety Administration (NHTSA) introduced the standards to reduce fuel consumption and GHG emissions. The standards are aimed at improving fuel economy of heavy- and medium-duty trucks, buses, and commercial pickups and vans (USEPA, 2011). The adoption of the first phase of standards will be phased in from 2014-2018 and seeks to reduce GHG by nearly 250 million metric tons and 500 million barrels of crude oil (USEPA, 2011). Deliberations toward a second phase of heavy-duty vehicle standards for 2020 and beyond have begun (White House, 2014), further motivating questions about technology potential, availability, and cost.

With the recent focus on fuel economy and GHG emissions, regulatory agencies are increasingly relying on vehicle simulation tools that allow the prediction of fuel consumption and GHGs for a variety of vehicles over different test cycles. The heavy-duty fleet is very diverse in both vehicle configuration and activity patterns, so the use of simulation makes strong practical sense for reducing the time required for fuel economy testing. In the U.S., the Greenhouse Gas Emission Model (GEM) is helping regulatory agencies as a regulatory tool. While in Europe, the VECTO model, will serve as the regulatory CO_2 emissions reporting tool.

Simulation tools such as Autonomie developed by Argonne National Laboratory and IGNITE by Ricardo, have become widely accepted methods to predict vehicle fuel consumption from a combination of engine, powertrain and chassis design features. These simulation tools have afforded researchers and regulators the ability to model an entire vehicle based on component block models and to further exercise the vehicle simulation over different vehicle driving cycles. One of the salient features of such physics-based models is that the flow of energy through the various subsystems can be visualized to better understand the losses and energy recovery systems that possibly affect fuel economy. Vehicle simulation models offer the capacity to change vehicle parameters that affect the road load equation and auxiliary loading systems in vehicles to understand their effects on fuel consumption without elaborate experimental test procedures. The accuracy of the prediction, however, is directly dependent on the accuracy of the model blocks that represent the various components of the vehicle. For instance, the accuracy of the road load on a vehicle is direct manifestation of the real-world aerodynamic drag area, vehicle weight, and tire rolling friction inputs.

Of the many components of a vehicle simulation model, the engine fuel map as a function of speed and torque is vital to calculate fuel consumption when simulating driving cycles. The accuracy of the fuel map in reflecting real-world engines will contribute to a representative fuel consumption profile of a vehicle.

The West Virginia University (WVU) Center for Alternative Fuels, Engines and Emissions (CAFEE) collaborated with the International Council for Clean Transportation (ICCT) to quantify the efficiency, energy losses, and prospects for efficiency improvements in diesel engines for heavy-duty vehicles. The project entails experimentally characterizing accurate fuel maps of representative US EPA 2010 compliant heavy-duty and medium-duty diesel engines. The developed fuel maps serve as inputs for the engine block in Autonomie for complete vehicle and powertrain simulation. The global objective of the study is to accurately estimate the fuel efficiency of US EPA 2010 heavy-duty diesel vehicle using Autonomie and further analyze 2017 and future heavy-duty fuel efficiency by considering technology advancement associated with the powertrain.

The specific objectives of the study are as follows:

1) Characterize the fuel map of two US EPA 2010 compliant diesel engines using engine dynamometer testing and conduct an energy audit to quantify their energy losses.
2) Utilize the data and underlying detailed energy audit analysis of the US EPA 2010 compliant engine with technology predictions to develop a fuel map for an engine that is representative of US EPA and NHTSA 2017 GHG and fuel efficiency standards.
3) Assess the potential for advanced energy efficiency technologies for the 2020-2030 timeframe and provide a fuel map and a detailed energy audit for an engine that incorporates those technologies.
4) Develop a waste heat recovery (WHR) simulation based on energy flows from the energy audit conducted on the US EPA 2010 engine.
5) Analyze the differences between engine operation in steady-state and transient conditions to approximate a transient correction factor to estimate the difference at various engine load points.

1.1 Background

1.1.1 Simulation Modeling of Fuel Consumption

Detailed engine models such as GT-Power can generate high fidelity simulation results. In these models, engine performance can be characterized at crank-angle resolution. These combustion-level models have the ability to capture transient phenomena like turbo lag or precise injection timing. GT-Power offers an intermediate step namely “Fast Running Model” which simplifies many of the flow paths but retains a crank-angle resolution of the engine performance parameters. This model runs significantly faster than a detailed engine model (close to real time) but must be tuned for the operating range in order to accurately reflect the detailed engine. Engines can also be modeled using performance maps that describe the operating characteristics of the engine across the speed-load range. This map-based engine can be simulated using vehicle simulation software such as Autonomie where the power demand to the engine is described as a continuous function of vehicle and duty cycle parameters. A map-based model is computationally inexpensive and is very well suited for studies such as drive cycle analysis or fuel efficiency calculation to capture vehicle-level phenomena with a substantial reduction in computational time.

1.1.2 Engine Transient Phenomena

An engine’s transient performance depends on various design features adopted by the OEM. For instance, the design and calibration of the Variable Geometry Turbocharger (VGT) dictates the type of throttle response that engine will produce. Engine manufacturers emphasize on performance, emissions and aftertreatment activity as primary transient operation criteria. Hence, significant differences can be

observed between extended steady-state operation and transient activity. OEMs strive to achieve the best possible fuel economy within regulatory standards and as a result include subtle differences in their technology and control strategy.

Distribution of energy losses change continuously during transient engine operation and the monitoring of the energy distribution on a temporal resolution is highly challenging. Changing DPF soot loading and desired EGR mass flow rates contribute to variations in pumping loss of the engine, further auxiliary devices such as the water pump, oil pump and fuel pump act as variable parasitic losses across the engine lug curve. The thermodynamic state of the engine and oil also affect the lubrication and convective and radiative heat transfer from engine surfaces. Therefore, data driven energy distribution models for different regions of the lug curve are needed to characterize the flow of energy as a function of speed and torque.

1.1.3 Engine Efficiency and Loss Mechanisms

Figure 3 illustrates a hypothetical energy audit for an engine over a particular operating condition. The proportion of the fuel energy[1] that is converted into indicated work (i.e. work done on the piston) is a direct measure of the engine's fuel conversion efficiency. Irreversibility during the combustion process (fluid friction, mixing, rapid expansion) affect the amount of work extraction by the piston, the energy leaving the engine cylinder as heat, and the energy remaining in the exhaust at the end of the expansion process. These indicated efficiency losses represent fuel energy that was not converted into work during the combustion process. Moreover, not all of the energy that is converted into work done on the piston makes it to the final engine shaft output. Some of the energy is used in overcoming engine friction at the bearings and piston-cylinder interface, some is used to pump air into the engine and exhaust gases out of the engine (pumping losses), and some is used to power engine auxiliaries and accessories (e.g., water pump, oil pump, fuel pump, cooling fan, alternator, power steering fluid pump, compressor for cabin air conditioning). The brake thermal efficiency value, expressed as a percentage, is the ratio between the useful work at the engine shaft output and the fuel energy input. Note that it is common practice to exclude some accessories during engine testing and the excluded accessories may vary depending on the engine laboratory standard practices.

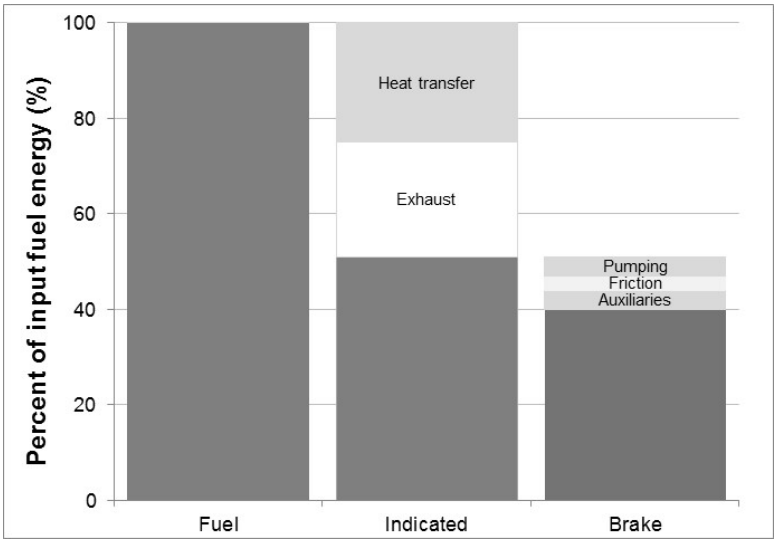

Figure 3. ***Energy loss mechanisms within an engine energy audit.***

[1] Fuel energy = fuel mass (kg) x fuel lower heating value (MJ/kg).

Figure 4 shows the historical changes in heavy-duty engine BTE mainly due to changes in emissions regulation and advancements in engine technology. The figure shows engine BTE over the FTP and UDDS cycles calculated from WVU's large database of engine and chassis dynamometer test data. The figure also displays historical values of peak BTE calculated from brake-specific fuel consumption presented by Volvo at 2011 DEER conference (Greszler, 2011). The figure shows the range of efficiencies that might be expected from differences in cycle characteristics and engine operational loads that change the magnitude and distribution of engine losses. Highest engine efficiency is not realized throughout transient cycles and operational characteristics affect the overall BTE of the engine. Even while US EPA regulations have reduced NOx and PM standards by over 95% between 1992 and 2010, heavy-duty engine have shown progress towards improved fuel efficiency, with the exception of the post consent decree (model year 2004) engines that show an approximate 6% decrease in BTE. This drop in engine efficiency could be related to the regulation by the US EPA to the OEMs to achieve a NOx standard of 2.4 g/bhp-hr from an earlier 1998 standard of 4.0 g/bhp-hr without the use of defeat devices. OEMs products achieved this emissions reduction without the use of any NOx aftertreatment systems. The pathway to this emissions reduction could have directly affected the engine efficiency during this period. Since then, a simultaneous improvement to engine and aftertreatment technology with a corresponding decrease in emissions have enabled OEMs to simultaneously develop more efficient and cleaner diesel engines.

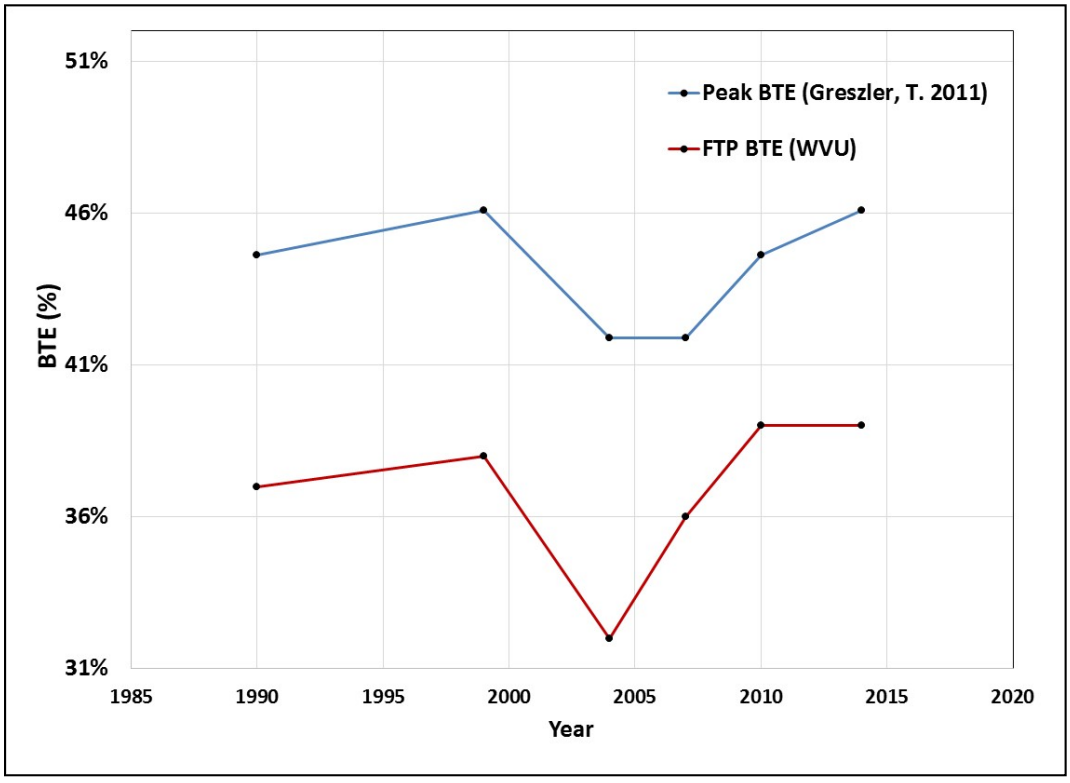

Figure 4 Historical changes in heavy-duty engine efficiency from WVU FTP and Volvo peak BTE (Greszler, 2011) data

1.1.4 Engine Model

Numerical models that simulate engine performance are vital to understand and predict the potential of

future engine technologies to improve engine efficiency. However, these models require a complex understanding of engine behavior and accurate design inputs to accurately predict engine energy flows. Modern heavy-duty diesel engines have multiple control algorithms that OEMs could potentially change depending on emissions compliance and fuel economy targets. Therefore, accurate data driven engine models are imperative for successful prediction of energy flows and fuel consumption of current and future heavy-duty diesel engines.

Simulation tools such as Autonomie do not require detailed engine models to predict fuel consumption. Autonomie works with a fuel look-up table for respective speed and torque to interpolate appropriate fuel consumption rates. Therefore, a data driven approach is necessary to develop these fuel map inputs for Autonomie to predict fuel economy on various real-world driving cycles. The primary goal of this project was to develop Autonomie fuel map inputs for US EPA 2010 compliant heavy- and medium duty diesel engines. The engine fuel maps will be integrated with suitable chassis parameters using the Autonomie tool, in order to predict representative fuel economy for various driving cycles.

A challenge in developing fuel lookup tables for Autonomie lies in the fact that, ideally, the adopted test procedure takes into account the possible effect of engine transients on the fuel consumption pattern. Factors such as EGR rate, water pump load, oil pump load, DPF soot loading, and VGT actuation could possibly create differences in actual fuel consumption while compared to values measured at steady-state conditions. Therefore, this study aimed to develop fuel map surfaces that fit measured fuel consumption rates of both steady-state operating conditions and transient acceleration and deceleration ramps. It must be noted however, that the risk of over-fitting the data with transient events could result in higher errors in fuel consumption prediction than when using pure steady-state data. Therefore, this study adopted a data collection and post-processing routine to avoid over fitting of the measured data.

2 TEST ENGINE SPECIFICATION

Two US EPA 2010 emissions compliant engines (12.8L Mack MP8 and 6.7L Cummins ISB) and one legacy US EPA 2004 emissions compliant engine (12.8L Mercedes Benz OMB 460) were tested on an engine dynamometer test bench to characterize their fueling maps and to quantify the different energy loss mechanisms through an energy audit. The 2010 compliant engines were the starting point for subsequent analysis to predict future 2017 and 2020+ engine fueling maps and energy audits. The 12.8L Mercedes Benz engine, being representative of a pre-aftertreatment technology, was useful to identify technology progression over the past decade, and to quantify the effects of the aftertreatment systems in the fuel consumption maps.

2.1 US EPA 2010-Compliant Heavy-duty Diesel Engine

In order to characterize the fuel map and energy audit for a US EPA 2010 compliant heavy-duty diesel engine, WVU tested a Mack MP8 505C. Table 1 shows the engine specifications. A technologically similar Volvo D13 engine was used to measure the indicated power of the engine since in-cylinder pressure measurement was available for the D13. The testing of the Volvo D13 was only conducted to correlate frictional power obtained from in-cylinder pressure measurement with friction power measured through motoring tests. The energy audit and fuel consumption measurements were performed on the Mack MP8 engine. Figure 5 shows the baseline 2010 Mack engine installed on the test cell.

Table 1. Engine specifications for USEPA 2010 heavy-duty diesel engine

Manufacturer	Mack
Model year	2011
Model	MP8 – 505C
Displacement (L)	12.8
Rated Horsepower (hp)	505
Rated Speed (rpm)	1800
Peak Torque @Speed	1810 ft-lb@1100rpm
Aftertreatment system	DPF-SCR
EGR	High pressure cooled EGR
Turbocharger	VGT
Fuel Injection	Electronic unit injectors (2400 Bar)
Compression Ratio	16:1
Bore and Stroke	131mm and 158 mm

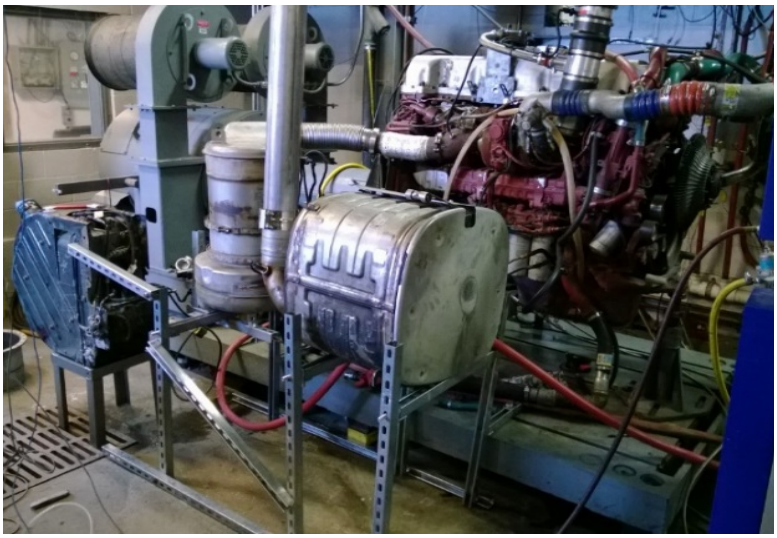

Figure 5. Mack MP8 505 C equipped with DPF and SCR

2.2 Legacy US EPA 2004 Compliant Heavy-duty Diesel Engine

In order to understand the technology and fuel consumption progression from pre-2010 engines to current US EPA 2010 compliant engines, a Model Year 2005, Mercedes MBE 4000 engine was tested to evaluate its fuel map and energy audit. The engine is certified at 2.4 g/bhp-hr NOx and 0.1 g/bhp-hr PM, and does not operate with a DPF or a SCR system. Table 2 shows the engine specifications. Figure 6 shows the engine installed in the test cell.

Table 2. Engine specification of US EPA 2004 engine

Manufacturer	Mercedes-Benz
Model year	2005
Model	MBE 4000 OM 460
Displacement (L)	12.8
Rated Horsepower (hp)	386
Rated Speed (rpm)	1986
Peak Torque @Speed	1381 ft-lb @1080rpm
Aftertreatment system	None
EGR	High pressure cooled EGR
Turbocharger	VGT
Fuel Injection	Electronic unit injectors (2000 Bar)
Compression Ratio	17.75:1
Bore and Stroke	128mm and 166mm

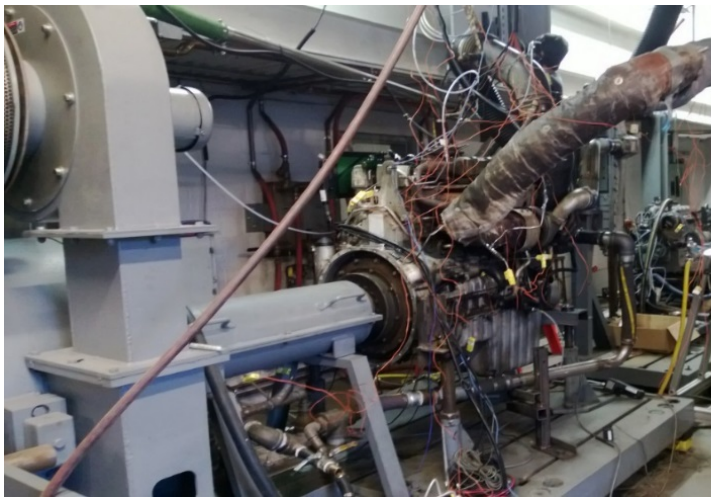

Figure 6. Mercedes OM460 386hp

2.3 US EPA 2010 Compliant Medium-Duty Diesel Engine

A model year 2013 Cummins ISB 6.7L was tested to characterize the fueling map and the energy audit of a US EPA 2010 compliant medium-duty diesel engine. Table 3 lists the engine specifications. Figure 7 shows the test cell setup of the Cummins engine.

Table 3. Engine Specification of USEPA 2010 Medium-duty Engine

Manufacturer	Cummins
Model year	2013
Model	ISB 6.7
Displacement (L)	6.7
Rated Horsepower (hp)	325
Rated Speed (rpm)	2400
Peak Torque (ft-lbs) @ Speed	750@1600 rpm
Aftertreatment system	DPF-SCR
Turbocharger	VGT
EGR	High pressure cooled EGR with intake throttle valve for pumping loss reduction
Fuel Injection	High Pressure (1800 Bar) Bosch CP3 Common rail fuel injection
Compression Ratio	17.3:1
Bore and Stroke	107 and 124 mm

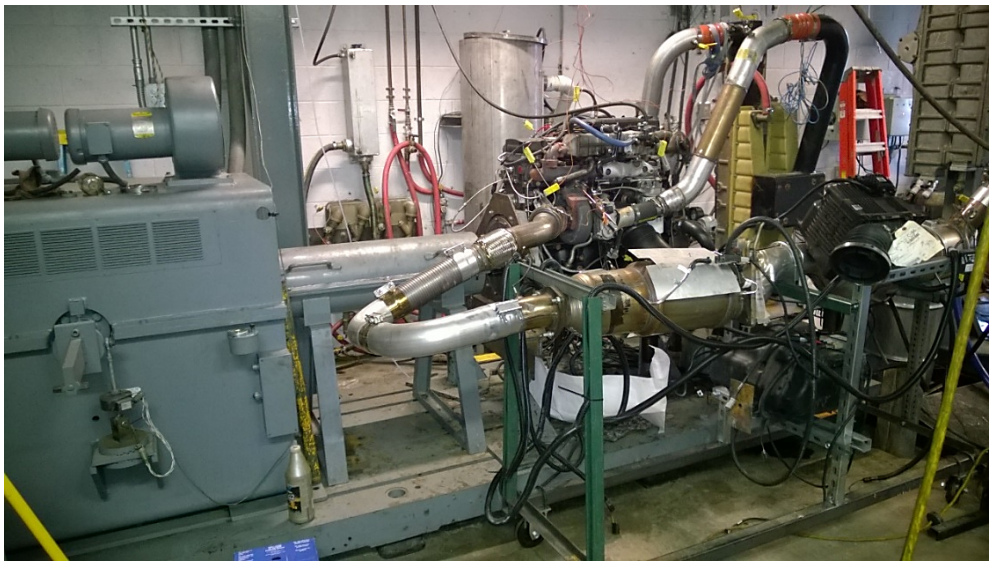

Figure 7. MY 2013 Cummins ISB 6.7 equipped with DPF and SCR

3 EXPERIMENTAL SETUP

Engine dynamometer experiments were performed at WVU CAFEE's §40 CFR 1065 compliant Engine Research Center (ERC) in Morgantown, WV. WVU CAFEE is equipped with two DC dynamometers (800 HP and 400 HP) and one AC dynamometer rated for 280 HP. The engine testing for the heavy-duty platform was conducted on an 800 HP DC dynamometer capable of engine speeds up to 2500 RPM. The medium-duty engine testing was performed on a 400 HP DC dynamometer capable of engine speeds up to 2900 RPM. Engine installation in the test cell involved the adaptation of the engine flywheel to a dynamometer shaft that connects the engine and DC dynamometer. WVU CAFEE's in-house engine dynamometer test cell software was used to provide throttle input and speed control of the dynamometer.

The heavy-duty engine was installed in the test cell with its aftertreatment system. As shown in Table 4, the cooling fan, alternator and other components were not part of the engine auxiliary devices in the test cell. While all of these auxiliaries are expected to consume power while in-use (power consumption will be heavily dependent on vehicle duty cycle), these components are not consuming power during the engine dynamometer testing and therefore are excluded from the engine fueling map and energy audit. On the other hand, the power consumption of some engine related auxiliary components that are essential for engine operation such as water, oil and fuel pumps are measured during the test, and are already implicitly covered by the resultant fueling maps.

Table 4. Engine Auxiliaries Included and Excluded During Engine Fueling Map Testing

Included (accounted for in the map)	Excluded (not accounted for in the map)
Water pump	Cooling fan
Oil pump	Alternator
Fuel pump	Air conditioning compressor
	Air compressor
	Power-steering pump
	Power take-off

3.1 Test Cell Integration

The heavy-duty Mack MP8 505C engine was removed from a Class 8 tractor and installed in the test cell. Since the engine in the truck interfaces with multiple vehicle components, it was necessary to procure a wiring harness and to connect the engine control unit (ECU), aftertreatment ECU and the test cell control. In addition, the engine and aftertreatment systems communicate with each other and with the vehicle interface through a separate controller area network (CAN) bus. Therefore, the engine required certain vehicle specific parameters such as ambient temperature, vehicle speed and ECU clock be provided by the test cell computer for proper functioning of the engine and aftertreatment system. Volvo North America supported the study by providing the necessary CAN messages and procedures to complete the integration of the engine in the test cell. With the complexity of aftertreatment integration, it was important to ensure that the engine was able to communicate with all units of the aftertreatment system, in order to prevent engine de-rate and possible non-representative open loop fuel control. The DPF and SCR were used in the state that they were when removed from the engine and no regeneration was performed prior to testing. Literature shows that a typical DPF provides a differential pressure of approximately 5 kPa while clean and 10 kPa during loaded conditions at rated exhaust flow rate conditions (Tan et al., 2011).

The Cummins ISB6.7 was provided by Cummins Inc. as test a cell ready engine with all necessary components, wiring harness and detailed test cell integration procedures.

4 TEST PROCEDURE

The test procedure was aimed at characterizing the fuel consumption and the energy flows in a heavy- and medium duty diesel engines. The engine instrumentation, testing procedure and modeling methodology are explained in this section.

4.1 Engine Instrumentation

Figure 8 shows the schematic of the instrumentation installed on the test engines. In order to estimate the energy flows in the air, exhaust, coolant, and oil streams, thermocouples were installed on all fluid flow pathways. Intake air mass flow rate, coolant flow rate and exhaust flow rate were also measured. The EGR circuit was instrumented with thermocouples before and after the EGR cooler to assess the change in enthalpy of EGR gases across it. All data channels where recorded at a frequency of 10 Hz. The engine instrumentation also included the aftertreatment system, however, the control volume for the energy audit was restricted only to the outlet of the turbocharger.

The fuel flow measurement for the study was measured using an AVL fuel flow meter. The AVL fuel flow meter and conditioning system measures instantaneous fuel flow measurement using the Coriolis principle. The fuel flow meter is capable of fuel flow and density measurements with an accuracy of 0.12%. In addition to the AVL fuel flow measurement, ECU-reported fueling was recorded.

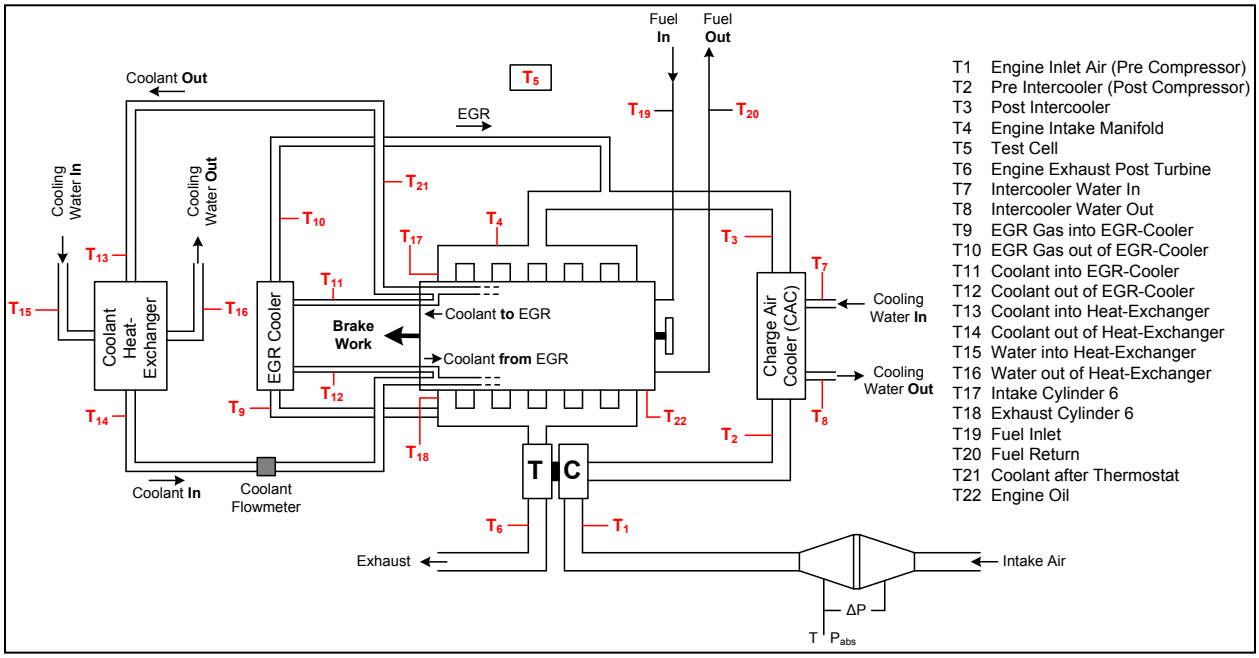

Figure 8. Schematic of engine instrumentation

In order to calculate the EGR fraction at the intake manifold, WVU adopted an enthalpy balance principle assuming adiabatic fluid mixing. This calculation required temperature measurements of intake manifold, post-CAC air, and the post-EGR cooler gas.

$$\dot{m}_{egr} = \left| \frac{\left((C_p(\mathrm{T}) * T)_{intakemanifold} - (C_p(\mathrm{T}) * T)_{intakeair}\right)}{\left((C_p(\mathrm{T}) * T)_{egr} - (C_p(\mathrm{T}) * T)_{intakemanifold}\right)} \right| * \dot{m}_{intakeair}$$

Where

Cp(T): Specific heat of gas at respective temperature T [kJ/Kg.K].

$T_{intakemanifold}$: Temperature of charge air post CAC and EGR mixer [K].
$T_{intakeair:}$ Temperature of intake air to compressor side of turbocharger [K].
$T_{egr:}$ Temperature of EGR [K].

In the equation, heat capacity (Cp) values for the EGR gases were assumed to be those of air at respective temperature and pressure conditions. Heat capacity values were obtained through NIST Reference Fluid Thermodynamic and Transport Properties Database (REFPROP) Version 9.1.

The method of determining EGR fractions through an adiabatic mixing assumption is widely used in the industry to validate EGR flow measurement devices in the engine. Other methods of EGR calculation include the use of oxygen sensor and CO_2 measurements that were not available for this study.

4.2 Engine Lug Curve

Engine mapping procedures were used to measure the peak torque and peak power curves of the engine as a function of engine speed. Engine mapping is important to understand the proper functioning of all components of the engine in order to deliver the peak torque and power specified on the engine tag.

The engine was warmed to stabilize the coolant and oil temperatures prior to the procedure. WVU test cell software tracks the engine coolant and oil temperature to determine stability to begin the engine mapping procedure. Upon stabilization the control software performs a wide-open-throttle (WOT) (i.e., 100% throttle) sweep over the engine speed range (i.e., from idle to governed speed) continuously increasing the speed at a rate of 4 rpm/s. Three consecutive tests are performed to validate the final torque and power curves. These curves are also used as upper boundaries for the fueling mapping process and are required inputs for the engine dynamometer test bench to run test cycles.

4.3 Motoring Procedure

The engine was also subjected to a motoring procedure with no fueling in order to characterize the frictional torque of the engine. The motoring map provides the frictional and pumping losses associated with the different engine speeds. It is to be noted that since this map is performed under no fueling conditions, the motoring curve will not reflect the additional friction imposed by the piston rings during actual in-cylinder combustion (where the cylinder pressures are orders of magnitude higher). The characterization of the actual in-cylinder friction during combustion can be performed only with in-cylinder pressure measurements. The difference in indicated power measured from in-cylinder pressure measurement and brake power will result in the actual frictional and pumping loss power that are experienced by an engine during combustion events. WVU employed in-cylinder pressure measurement for MY 2005 Mercedes engine and the Volvo D13. The exhaust backpressure for the Volvo D13 was set to the values observed on the Mack MP8 at rated power (110 kPa absolute pressure). The exhaust backpressure setting will effectively simulate the pumping loss of the aftertreatment system. The Cummins ISB 6.7 and the Mack MP8 505C, however, did not have provisions for in-cylinder pressure measurement. For these engine platforms, it was decided to use the summation of brake power and frictional power to obtain the indicated power of the engine.

4.4 Fuel Map Development

To efficiently cover the operational envelope of the engine, two different design of experiments (DOE) space filling designs (Gaussian and Latin Hypercube) were used to characterize the engine fuel consumption map. Description of the methods is provided in the Appendix. Each method provided 25 points under the lug curve for a total of 50 points. A test procedure covered 50 points through a random pathway between the points. This procedure was used to measure fuel consumption and energy audit parameters with a smaller test duration than using a Cartesian grid under the engine lug curve. Figure 9

shows the steady-state points covered under the lug curve of the reference 2010 heavy-duty engine. The test captured both steady-state fueling at the individual 50 points and transient fueling while moving from one point to another. In addition to the 50 points picked by the DOE methodology, three ESC points on the 100% load of the lug curve were added to measure peak fueling rates. Data collection was performed for 2 minutes at each point steady-state point. Since engine transients can induce differences in fuel maps obtained through only steady-state operation, the transient dataset obtained from the test procedure adopted in this study can be potentially used for producing correction factors for the steady-state fueling maps. Later in this report, comparison of fuel maps derived from steady-state test points only versus fuel map developed through a combination of steady-state and transient test points are discussed.

The Gaussian fitting process is computationally more involved than a simple 2nd order fit. Therefore, the Gaussian fitting process could be trained only using the steady state points (lesser training points). Since, this study required to compare the fuel maps created from both steady-state and transient test points it was decided to use a simple 2nd order fitting process (with less computational requirement than the Gaussian fit) to generate the fuel maps. This study generated two fuel maps, one, from fitting a second order surface through only steady-state points, and two, from fitting a second order surface through a combination of steady-state as well as transient test points. Later, these two 2nd order surface fuel maps were used to predict the fuel consumption over a transient FTP cycle to evaluate the differences in fuel maps created from two different approach.

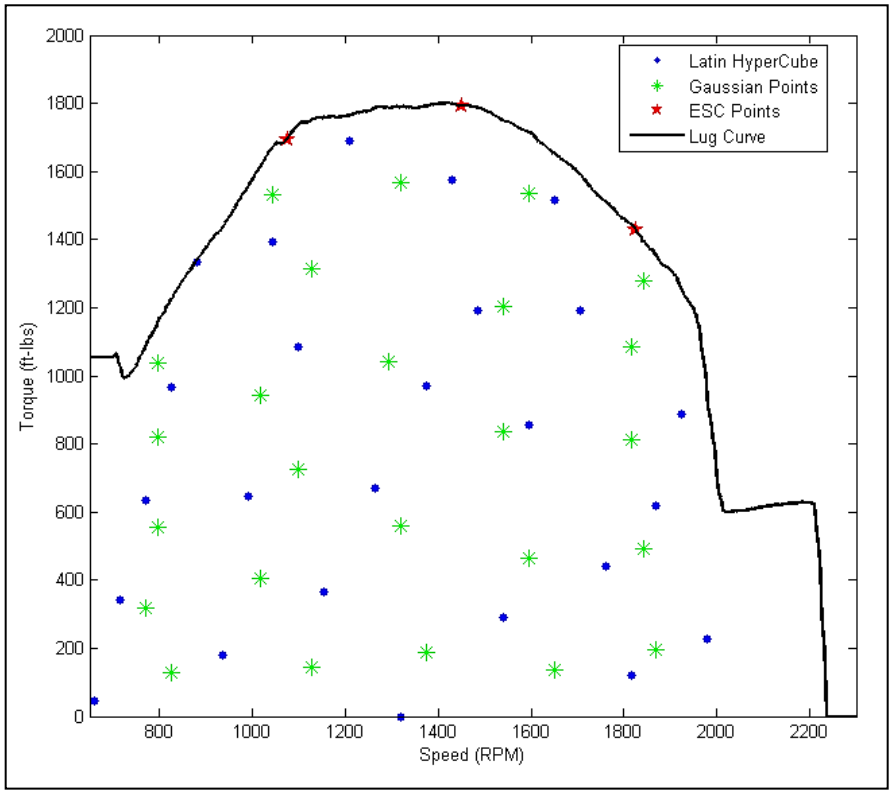

Figure 9. DOE test matrix with Gaussian and Latin Hypercube test points

It is to be noted that the fuel consumption characteristics measured for this study are representative of the engine operation on the test bench, under the conditions imposed by the engine dynamometer. Engine management strategies that include but are not limited to aftertreatment thermal management, extreme

ambient conditions calibration adjustments, DPF regeneration events, and fuel saving strategies during highway cruise driving are used by manufacturers during on-road operation and may be dependent on many other parameters and sensor feedbacks, which are not covered/controlled on the engine test bench. Hence, on-road fuel economy, similarly to emissions, can be different from engine dynamometer results.

Creating energy distribution maps under the entire operating range of the engine with only steady-state setpoints require the use of a robust fitting method rather than a simple 2^{nd} order fit. Therefore, the Gaussian fit procedure was used in this case to develop the energy audit map for the entire region under the lug curve. It is to be noted that unlike fuel consumption, the losses in an engine could be non-linear and as a result, accuracy of the loss prediction in certain regions of the lug curve could be lost. The use of Gaussian fitting process was aimed at minimizing this error. For example, combustion characteristics in a heavy-duty engine could be optimized in certain regions of the lug curve to provide optimum engine performance, and if the measured data did not capture the multiple regions in which the combustion is optimized, the model will fail to predict the combustion losses in those regions accurately. The prediction of losses accurately over the entire region of the lug curve will require extensive engine dynamometer testing to characterize the losses and efficiency at a finer resolution under the engine lug curve.

4.5 Energy Audit Methodology

Test engines were instrumented to measure temperature, pressure and flow rates of all fluid streams that transport energy to and from an engine. To characterize the energy losses and efficiencies a suitable control volume is needed. Figure 10 shows the chosen control volume that was bound to the outlet of the turbine on the exhaust side and the inlet of the compressor on the air intake side of the engine.

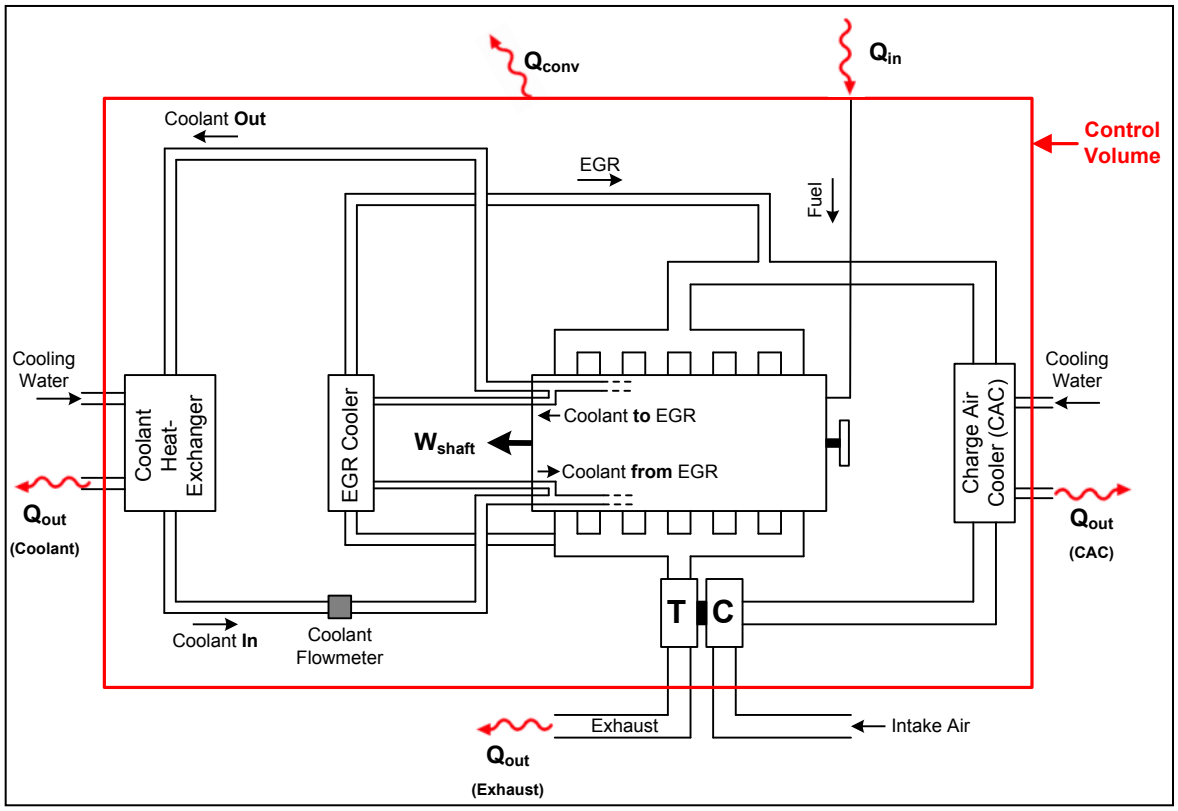

Figure 10. Schematic showing the engine control volume

Certain key assumptions are required to characterize the energy flows in an internal combustion engine:

1) The LHV of diesel fuel is assumed to be 42.8 MJ/Kg [*].
2) To evaluate the exhaust conditions and energy, the fluid assumed is air. Actual molar flow rate of emissions constituents would improve the accuracy of the energy audit, however, measurement of emissions was beyond the scope of the study.

Indicated power was measured using in-cylinder pressure measurement data for the Mercedes engine and Volvo D13. For engine platforms with no in-cylinder pressure (Cummins and Mack MP8), it was decided to use the summation of brake power and frictional power (from motoring test) to obtain the indicated power of the engine. Indicated power calculated through this procedure correlates well with indicated power measured using in-cylinder pressure data. Figure 11 shows the correlation of the indicated power measured using in-cylinder pressure measurement and calculated indicated power from the summation of measured brake power and frictional torque obtained from motoring tests. Frictional power of the engine will be evaluated using the motoring procedure at different engine speeds. Motoring tests were conducted in immediate succession to a hot engine mapping process in order to accurately capture the effect of lubrication oil viscosity and representative in-cylinder temperature conditions.

* *http://cta.ornl.gov/bedb/appendix_a/Lower_and_Higher_Heating_Values_of_Gas_Liquid_and_Solid_Fuels.pdf.* [Accessed 4/29/2014 2014]

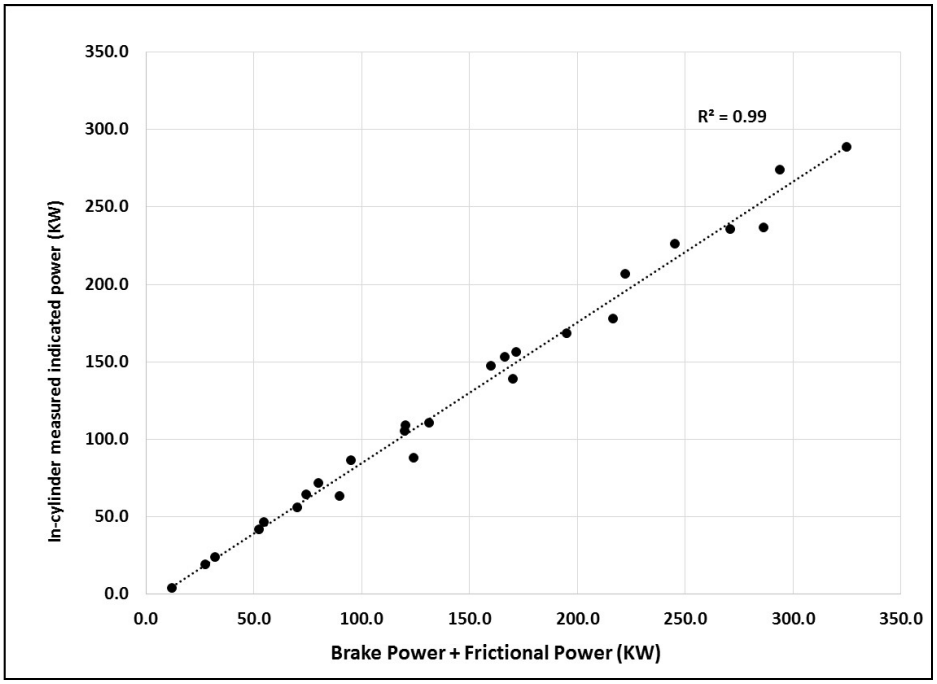

Figure 11. Scatter plot of in-cylinder measured indicated power vs calculated indicated power for the Volvo D13

The frictional power obtained experimentally through engine dynamometer procedure will include the combined losses of many factors, mainly

1. Oil pump work
2. Water pump work
3. Fuel pump
4. Unloaded air compressor work
5. Exhaust backpressure pumping losses
6. EGR related pumping losses as a result of VGT actuation
7. Frictional losses due to piston seal, bearings and lubrication oil viscosity

It is to be noted that although many parameters contribute to the total friction and pumping losses of a heavy-duty diesel engine, the frictional component of piston rings and bearings will be the significant contributor to the total loss at higher load conditions. Hence, the study reviewed data sheets and inputs from manufacturers to assess the individual energy consumption of oil pump, water pump and air compressor to decouple the energy consumption from the total friction and pumping work. The motoring tests may result in a lower frictional torque at higher loads, because the friction of piston seals and bearings during actual combustion will be significantly greater than during dynamometer motoring tests.

The decoupling of backpressure component was accomplished by conducting an experiment wherein the backpressure was varied for five different settings to measure the change in fuel consumption. For this purpose five hot engine tests were performed under different backpressure settings from 0.5 psig (3.4 kPa) to 4.5 psig (31 kPa) to discern the change in fuel consumption per psig change in engine backpressure. This task was performed on the Volvo D13 without the aftertreatment system in order to decouple the effect of changing soot loads in the DPF. The change in fuel consumption was later normalized as a percentage of total fuel energy to calculate the energy loss associated with engine backpressure.

4.6 Waste Heat Recovery Simulation

WVU developed a MATLAB simulation tool to model a waste heat recovery system based on an Organic Rankine Cycle (ORC). The simulation is based on recovering waste heat from EGR cooling and coolant circuit using a suitable fluid identified from literature. The simulation makes key assumptions based on literature findings and good engineering judgment. The fluid properties are obtained from REFPROP manager developed by NIST. The key assumptions for this simulation are given in Table 5. The working fluid was assumed as R245fa based on Cummins WHR system (Nelson, 2008b), rather than an ethanol system described by Park et al.

Table 5. List of Key Assumption in WVU WHR ORC Model (Park et al., 2011, Teng et al., 2011, Nelson, 2008b)

Primary Working Fluid	R245fa
Pump head	2068 kPa
Pump Efficiency	85%
Turbine Efficiency	85%
EGR Heat Exchanger Effectiveness	NTU method
EGR gas properties	Air properties assumed
Engine Coolant Heat Exchanger Effectiveness	90%
Mass flow rate of Working Fluid @ each mode	Based on Cummins ORC specifications (between 0.3 and 0.8 kg/sec)
Expander out Pressure	101.3kPa
Condenser out State	25°C Saturated Liquid State

OEMs have developed different kinds of WHR systems as part of the SuperTruck DOE project. The system developed by Cummins Inc. has been widely published and a wealth of literature is available for model assumptions. Therefore, WVU adopted a simulation pathway similar to the design developed by Cummins Inc. The simulation also assumes design parameters, such as turbine expansion ratio and generator efficiencies are based on good engineering judgment, and provides them as user inputs to study the energy recovery potential from the cycle. The salient feature of the simulation is that the model will use measured temperature and flow data of the various streams to study the energy recovery potential. Therefore, this model will provide a realistic estimate of the possibility and magnitude of WHR potential over the operating region of the engine. Figure 12 shows the schematic of the WHR ORC system simulated in this study. The schematic also shows the heat transfer regions between the working fluid and engine fluids.

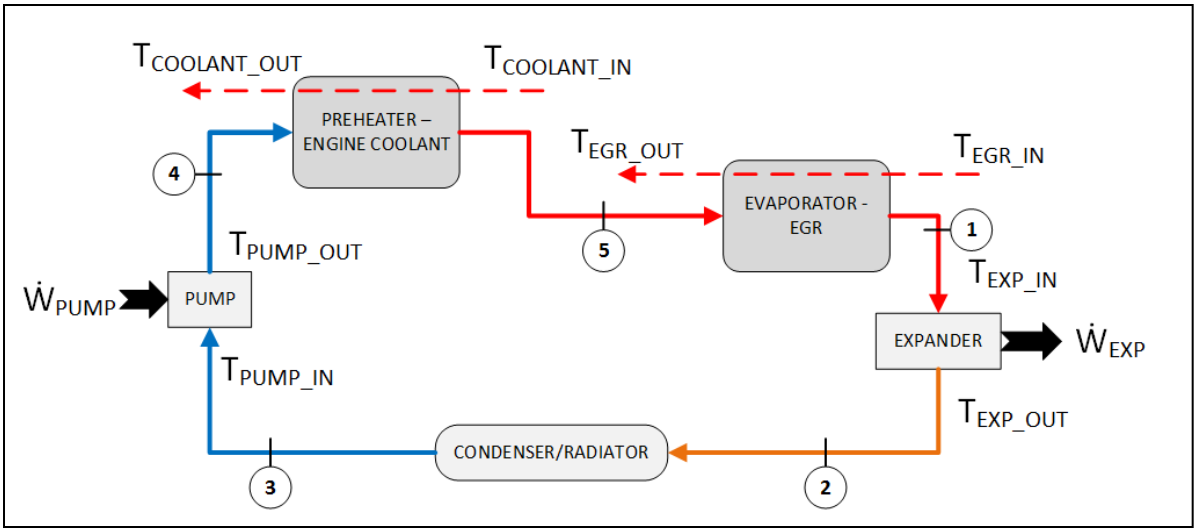

Figure 12. Schematic of ORC with energy recovery from EGR and Engine Coolant

The model of the ORC system consists of five major components -pump, pre-heater, evaporator, expander and condenser. Each sub-system and the processes are described below:

1) **Feed Pump:** For increasing working fluid pressure and generating the desired working fluid flow rate, pump properties based on Cummins (Nelson, 2008b) were chosen. A feed pump characterized to deliver 2068 kPa of pressure head and mass flow rate ranging from 0.3–0.8kg/sec. The fluid entering the pump at state 3 was selected to be at a saturated temperature of 25°C, as can be referred to the T-s and P-v diagram in Figure 14. The pump pressurizes the fluid with the constant provided pump head with a minimum increase in temperature and to a pressure of 2216.7kPa to state 4. The condenser out temperature is an assumption of an ideal Rankine cycle condition that considers a saturated fluid condition at both the inlet of the condenser and the boiler.
2) **Preheater – Engine Coolant:** The model utilizes the engine out coolant circuit heat transfer for preheating the working fluid entering at state 4. The energy recovered from the coolant helps the working fluid to reach a higher temperature at the given pressure level to state 5. Heat transfer highly depends on the mass flow rate of the working fluid flowing through the heat exchanger. The simulation model however considers different flow rates with a condition that the working fluid achieves vapor state at the outlet of the evaporator. The heat exchanger selected in our preheater analysis is a counter- flow shell and tube heat exchanger with an assumed effectiveness of 90% and with a negligible pressure drop through the system.
3) **Evaporator – EGR Cooler:** The preheated working fluid at state 5 passes through the evaporator heat exchanger utilizing the exhaust gas recirculated heat from the engine. Vaporization of the working fluid was only seen to be achievable with the implementation of the preheater and lower mass flow rates of the working fluid. The model selects a mass flow rate of the working fluid for the entire system based on the major requirement that the thermodynamic condition of evaporator out at state 1 is always at single phase vapor region. This avoids the state of the working fluid before the expander entering as a two-phase mixture region the heat exchanger selected in our evaporator analysis is a counter- flow shell and tube heat exchanger with exchanger effectiveness calculated based on NTU method. The pressure drop was assumed insignificant for the evaporator heat exchanger.

4) **Expander:** The vaporized working fluid at state 1 is expanded to a lower pressure of the system cycle which was selected to be the condenser pressure at 101.3kPa. The expander isentropic efficiency is assumed constant and equal to 85%. One of the main reasons for the choice of R245fa is that the working fluid is capable of phase change at relatively lower temperatures and expands while remaining in the gas phase after the expander. This property of R245fa makes it an ideal WHR fluid for internal combustion engines. Industry has also accepted R245fa as a safe working fluid that is environmentally safe, without causing ozone formation. Figure 13 shows example pressure-specific volume and temperature-entropy diagrams for R245fa simulated for WHR operation at a steady-state engine operation. It can be seen that upon isentropic expansion R245fa remains in superheated state, thereby preventing turbine cavitation. In addition, R245fa has shown best isentropic-efficiency at temperatures between 380 and 400 K. The fluid also has a maximum temperature limit of 500 K (Mago et al., 2006). Hence, the simulation also uses the temperature limiting condition to decide the mass flow rate of working fluid that will prevent working fluid decomposition.
5) **Condenser:** The working fluid from the expander at state 2 is introduced to the condenser at constant pressure and cooling process takes place rejecting heat to the environment through the condenser heat exchanger. For the model's standard assumption, the condenser-out reaches saturation state at selected temperature of 25°C at state 3.

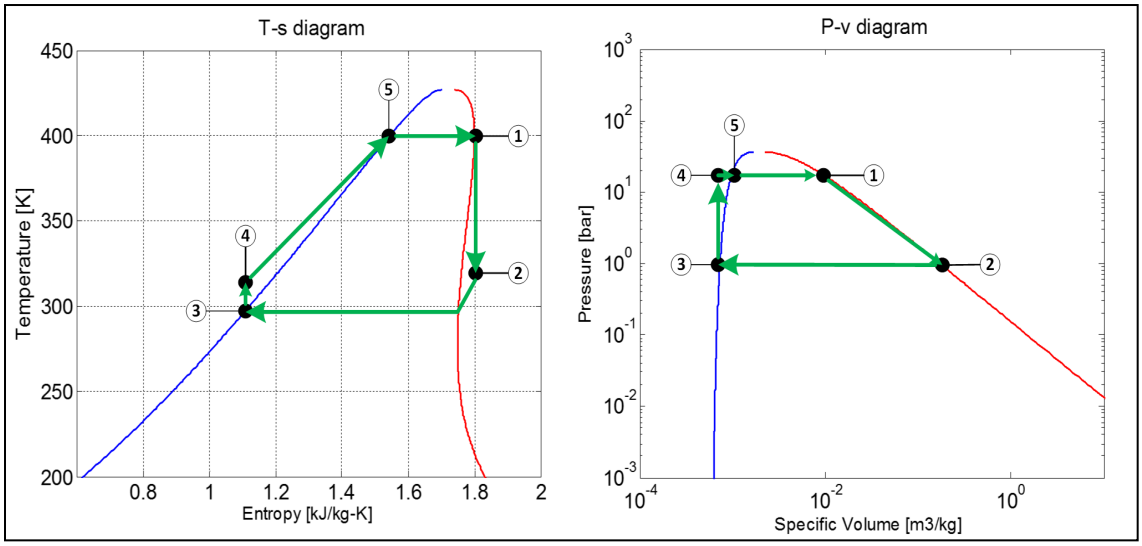

Figure 13. T-S & P-v diagram of the simple R245fa Rankine cycle WHR thermodynamic steady-state model

5 RESULTS

5.1 Fuel Map Characterization

5.1.1 MY 2005 Mercedes OM460

Figure 14 shows the fuel consumption contours under the operating curve of the Mercedes OM460 engine. The dots shown under the lug curve depict the test points generated by the DOE test matrix for the Mercedes engine mapping procedure. Figure 15 shows the fuel consumption rate predicted using the Gaussian model plotted with the measured fuel rate over the FTP cycle.

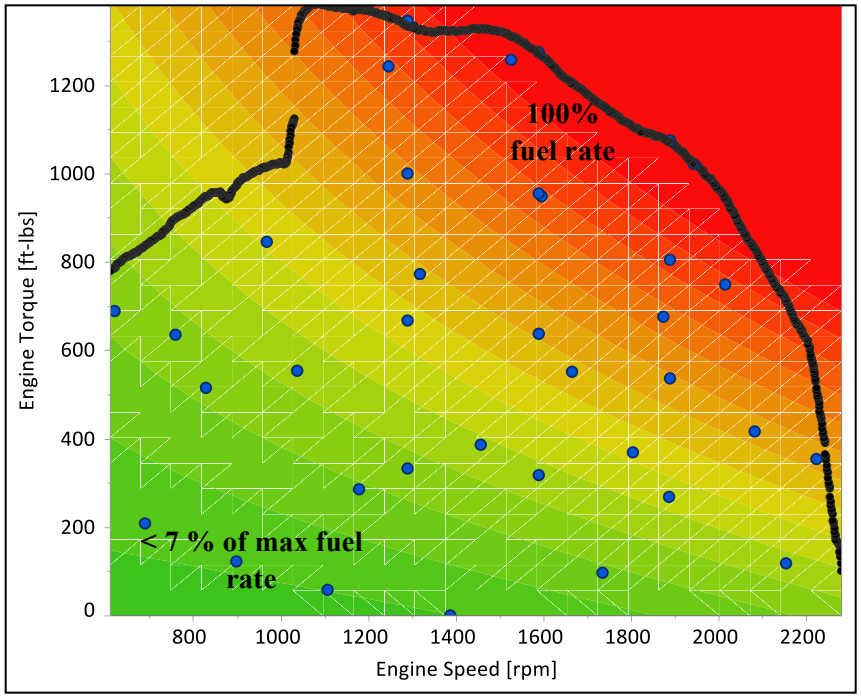

Figure 14. Contour plot prediction for Mercedes OM460 fuel flow rates [g/s].

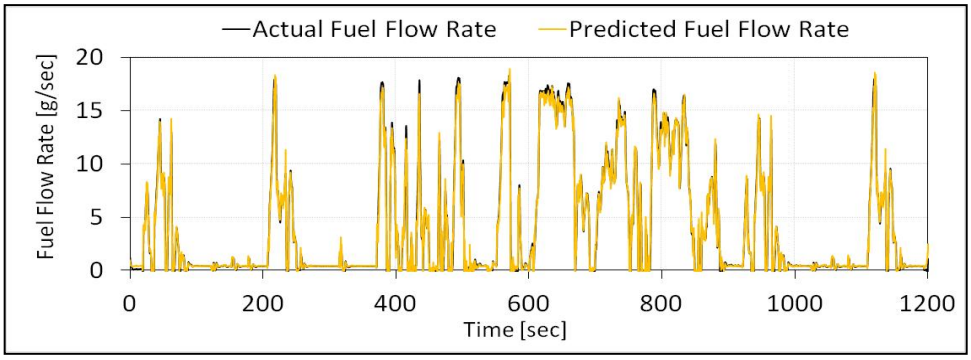

Figure 15. Predicted vs Measured Fuel Flow Rate for Mercedes OM460 on FTP cycle

Figure 16 shows the linear fit between the predicted vs measured fuel rate of the Mercedes OM460 over the FTP cycle. The total cycle fuel in grams and the statistics of the fit are tabulated in Table 6.

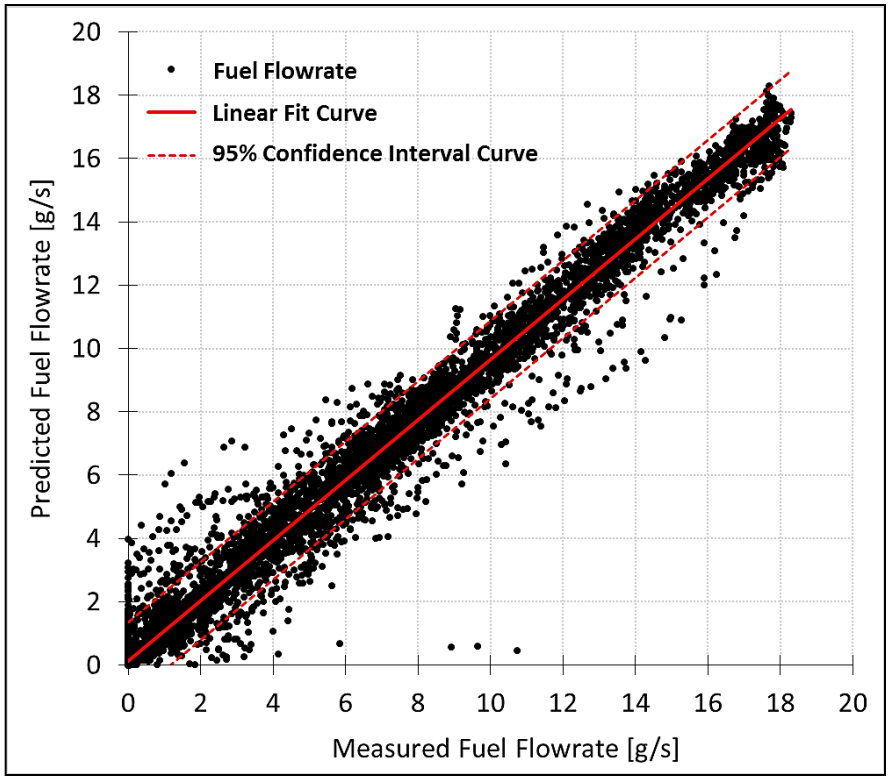

Figure 16. Scatter Plot of Fuel Flow Rate for Mercedes OM460 using the Gaussian Process Fit over FTP

Table 6. Summary of Linear Fit for Mercedes OM460 over FTP for the Gaussian Process Fit

Total FTP Cycle Fuel	
Actual Total Fuel [g]	4997
Predicted Total Fuel [g]	4943
Percentage error of integrated fuel	1.1%
Total FTP Work (kW-hr)	21.1
Summary of Linear Fit	
RSquare	0.9856
Root Mean Square Error	0.6242
Mean of Response	4.06
Number of Data Points	12090

Table 6 shows the statistics of the Gaussian fit used to predict the fuel consumption rate of the MY 2005 Mercedes over the FTP cycle. The error in integrated fuel consumption was calculated to be 1.1%, with a lower bias towards the prediction.

5.1.2 MY 2011 Mack MP8 505C

Figure 17 shows the fuel consumption contours under the operating curve of the US EPA 2010 compliant Mack MP8 engine. The dots shown under the lug curve illustrate the test points generated by the DOE test matrix for the Mack MP8 engine mapping procedure. Figure 18 shows the fuel consumption rate predicted using the Gaussian model plotted with the measured fuel rate over the FTP cycle. Figure 19 shows the fit between the measured and predicted fuel rate for Mack MP8 engine over the FTP cycle.

Table 7 lists the statistics of the fit between total measured and predicted fuel consumption in grams over the FTP cycle for the Mack MP8 engine.

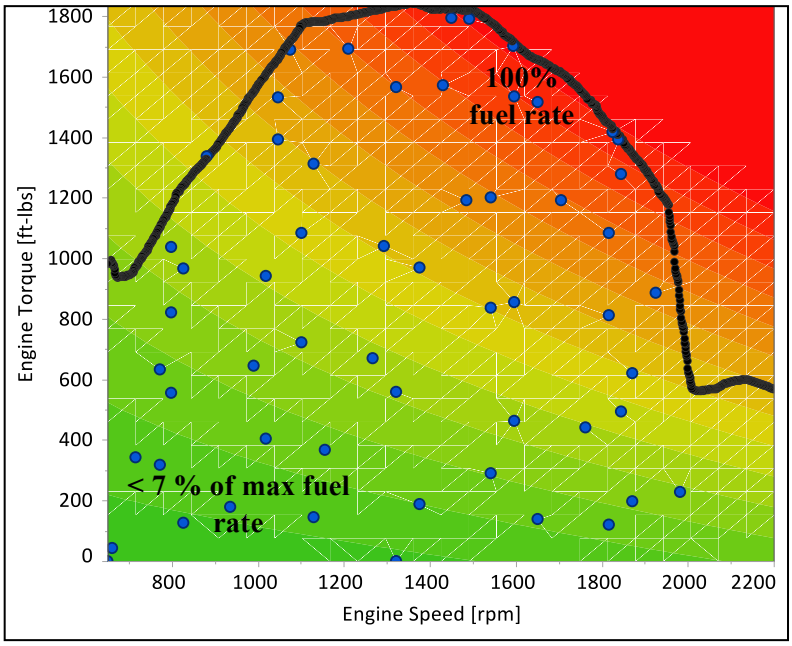

Figure 17. Contour plot prediction for MY2011 Mack MP8 fuel flow rates [g/s]

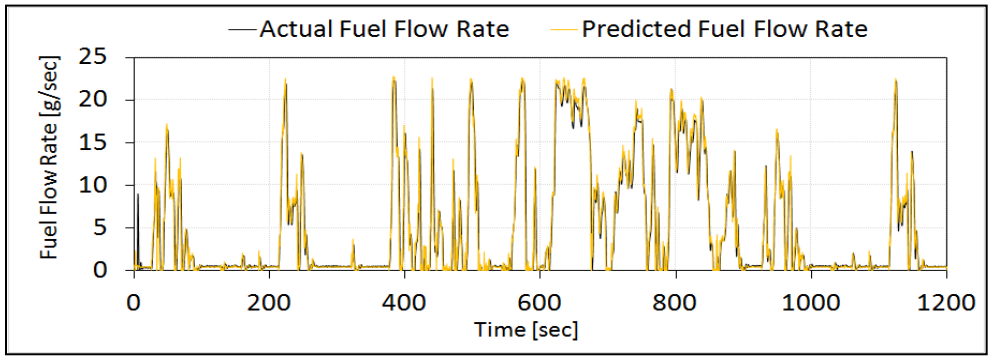

Figure 18. Predicted vs Measured Fuel Flow Rate for MY2011 Mack MP8 on FTP cycle

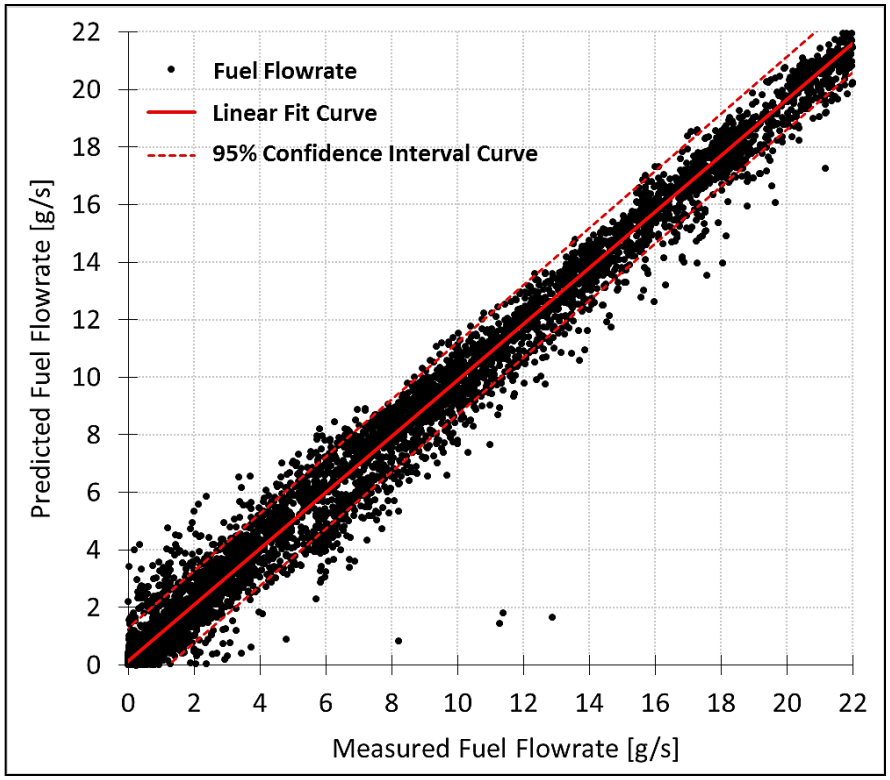

Figure 19. Scatter Plot of Gaussian prediction vs measured fuel flow for Mack MP8 over FTP

Table 7. Summary of Linear Fit for Mack MP8 over FTP

Total FTP Cycle Fuel	
Actual Total Fuel [g]	6228
Predicted Total Fuel [g]	6230
Percentage error of integrated fuel	0.01%
Total FTP Work (kW-hr)	25.9
Summary of Linear Fit	
RSquare	0.99087
Root Mean Square Error	0.646
Mean of Response	5.14
Number of Data Points	12090

5.1.3 Difference between steady-state and transient maps

Engine fuel maps can be developed either by collecting extensive real world data to surface fit the fuel consumption under the lug curve of the engine or conduct controlled steady-state tests over chosen points under the lug curve to measure fuel consumption accurately to further interpolate across the lug curve. Both approaches have their limitations leading to potential differences in estimating fuel consumption for speed or torque combinations not measured experimentally. Data from a highly transient engine operation will not provide stabilized fuel consumption at every point, as a result deviations in absolute magnitude of fuel consumption at a given point can be observed due to lack of a stabilized fueling event. Similarly, a simple steady-state test might not account for behavior under transient conditions of engine components such as water pump, oil pump, fuel pump and turbocharger and as a result may not accurately capture the rate of change of fuel consumption while moving between various speed and torque combinations.

To overcome these limitations, this study used a combined approach by developing a test cycle that contains a series of steady-state points with transient movements between the points. The fuel consumption is instantaneously recorded at 10 Hz during the course of the cycle. As a result, this test procedure yields both a detailed fuel consumption profile at 50 steady-state points and numerous transient points while moving between the steady-state points.

The study initially proposed to use the Gaussian process fit to train the fuel consumption data to populate the 25 x 25 fuel consumption matrix. Due to limitations of the statistical software of JMP in handling large datasets, the Gaussian process fit methodology was restricted to only predicting energy audit maps, while a simple 2nd order surface fit was used to create fuel maps for the heavy-duty and medium-duty engines. Figure 19 shows the prediction of a transient FTP cycle using the Gaussian process fit that was trained by using only the steady-state fuel consumption points of the test cycles. The results show that although, only steady-state points were used for training the data, the prediction of a transient FTP fuel consumption is accordance with measured fuel consumption rate over the FTP cycle.

In order to quantify the possible differences in fuel consumption profiles derived from steady-state testing versus a complete transient test cycle, a 2nd order surface fit (with less computational requirements than the Gaussian fit procedure) was used in JMP with two sets of training data. The first dataset used only the 50 steady-state test points to develop the 2nd order fit, while the second dataset used the entire dataset including the instantaneous fuel consumption measured while moving between the steady-state points.

Two 2nd order fit equations were derived from the datasets. Table 8 shows the summary of fit for the 2nd order equation developed using the transient and steady-state data points. A R^2 of 0.99 and root mean square error (RMSE) of 0.30 suggests a good surface fit of the data. Table 8 shows the summary of fit for the 2nd order equation developed using the transient and steady-state data points. A R^2 of 0.99 and root mean square error (RMSE) of 0.25 suggests a good surface fit of the data.

Table 8. Summary of fit for equation 1

RSquare	0.997
RSquare Adj	0.997
Mean absolute percent error	12.1%
Root Mean Square Error	0.303
Mean of Response	8.914
Number of Data Points	62999

Table 9 shows the summary of fit obtained for the 2nd order equation developed using only the 50 steady-state data points. The mean absolute percent error was calculated to be 19% in comparison to the 12.1% error obtained for the fit equation developed from Equation 1.

Table 9. Summary of Fit for Equation 2

RSquare	0.998
RSquare Adj	0.998
Mean absolute percent error	19%
Root Mean Square Error	0.259
Mean of Response	8.641
Number of Data Points	67

The two equations were then used to predict the instantaneous fuel consumption over the FTP to quantify the differences in the surface fit due to the steady-state and transient datasets. Figure 20 shows the scatter

plot between predicted fuel consumption and measured fuel consumption over the FTP cycle using both Equation 1 and Equation 2. The scatter plot illustrates the difference in fuel maps developed from surface fitting the data obtained from a complete steady-state testing versus data obtained from a combination of steady-state and transient test procedure. The fit obtained from both equation 1 and 2 resulted in a R^2 of 0.99 with a RMSE of 0.65 and 0.64 respectively. The statistics suggest minimal difference in fuel maps developed using steady-state and a combination of steady-state and transient dataset. Since both datasets are able to predict transient FTP fuel consumption to the same degree of accuracy, it can be concluded that no significant differences exists in using either of the dataset for training a fuel consumption model.

Further Equation 1 was used to populate the 25 x 25 Autonomie fuel matrix.

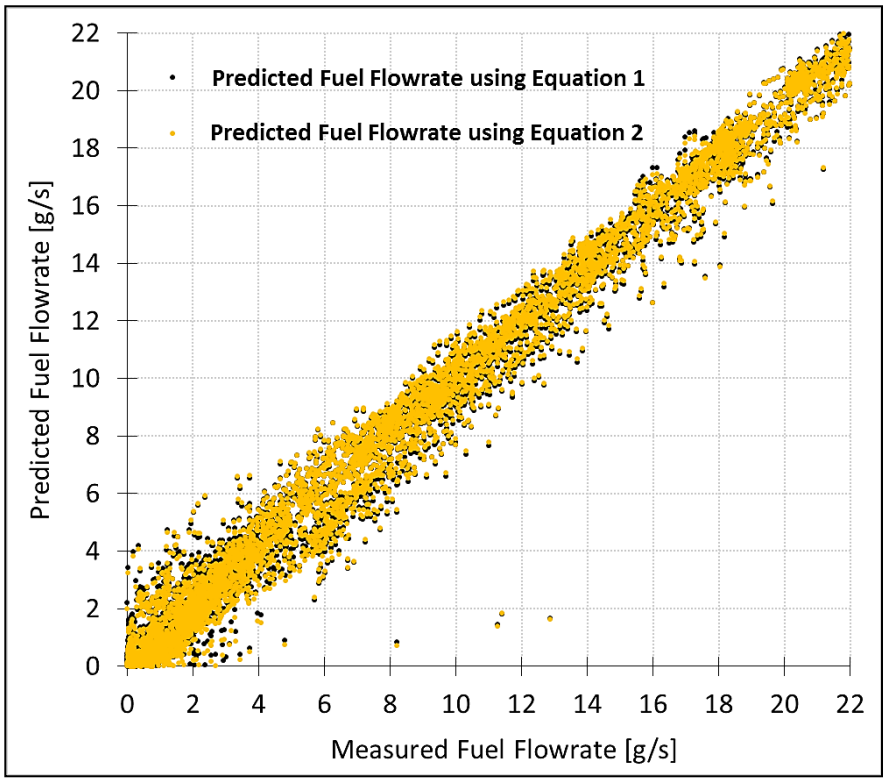

Figure 20 Actual Vs. Predicted Fuel consumption over FTP using 2nd order fits of Equation 1 and Equation 2

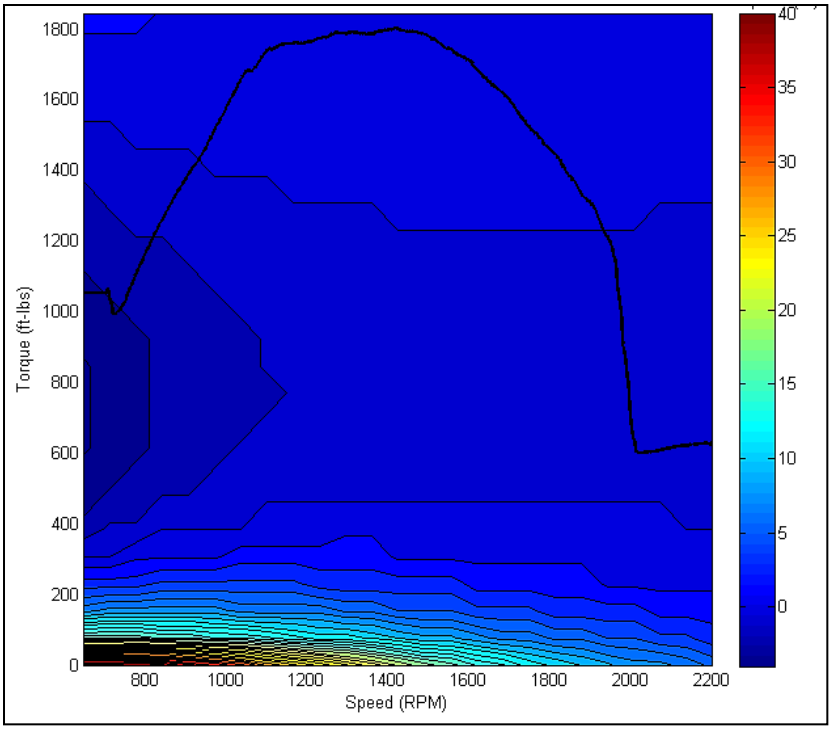

Figure 21 Percent difference in fuel map between steady-state and transient

Figure 21 shows the contour plots of the differences in fuel maps created from 2nd order fit of steady-state and transient engine operation data. The figure shows that the difference in fuel consumption populated using steady-state and transient data is found to be less than 2% for most regions of the lug curve. The large difference in fuel consumption observed at the lower loads of the lug curve is attributed to lower signal-to-noise ratios, and instability in engine loads at such low torque conditions contributing to high variations in measured fuel flow.

5.1.3.1 Transient Correction Factor

Depending on the dataset used for creating the fuel maps, possible differences can arise between fuel maps populated using steady-state and transient engine data. This differences are primarily due to the differences in losses between a stabilized engine operation and a continuously changing speed and torque characteristics. Since this study used both steady-state and transient data for populating the fuel map, it was important to calculate the differences in the fuel map developed using two different kinds of datasets. Therefore, two fuel maps using steady-state data and another using a combination of steady-state and transient fueling rates were created. The fit equations shown in Equation 1 (combination of steady-state and transient data) and Equation 2 (steady-state data only) were used to predict the fuel consumption over the FTP and SET cycles for the 2010 heavy-duty engine. Table 10 shows the difference predicted and measured integrated fuel consumption over the FTP and SET cycles. The prediction of the FTP fuel consumption using the transient data was 0.48% lower than the actual fuel consumed over the FTP. Similarly, the prediction over the SET showed a 0.9% higher bias for the predicted fuel consumption using the steady-state map and a 1% higher bias for the predicted fuel using the transient fuel map. Lower fueling rate during idle mode resulted in larger percent errors due to differencing of two small numbers, as result the idle point was not considered for the SET error estimation shown below. Based on the test procedure adopted in this study, the differences in fuel-maps are not very significant. This conclusion could be driven by the test methodology and the number of transient data points used to develop the fuel

maps. Fuel maps developed from real-world data collection with a larger dataset could show larger differences between steady-state and transient fuel-maps.

Table 10 Correction factor between steady-state and transient fuel maps

	Transient + Steady-state Prediction	Steady-state Prediction
FTP	-0.48%	-0.24%
SET	+1.0%	+0.9%

5.1.4 MY2011 Cummins ISB6.7

Figure 22 shows the fuel consumption contour under the operating curve of the US EPA 2010 emissions compliant Cummins ISB6.7 engine. The dots shown under the lug curve illustrates the steady-state points generated by the DOE methodology. Figure 23 shows the comparison of measured instantaneous fuel consumption versus predicted instantaneous fuel consumption over the FTP cycle.

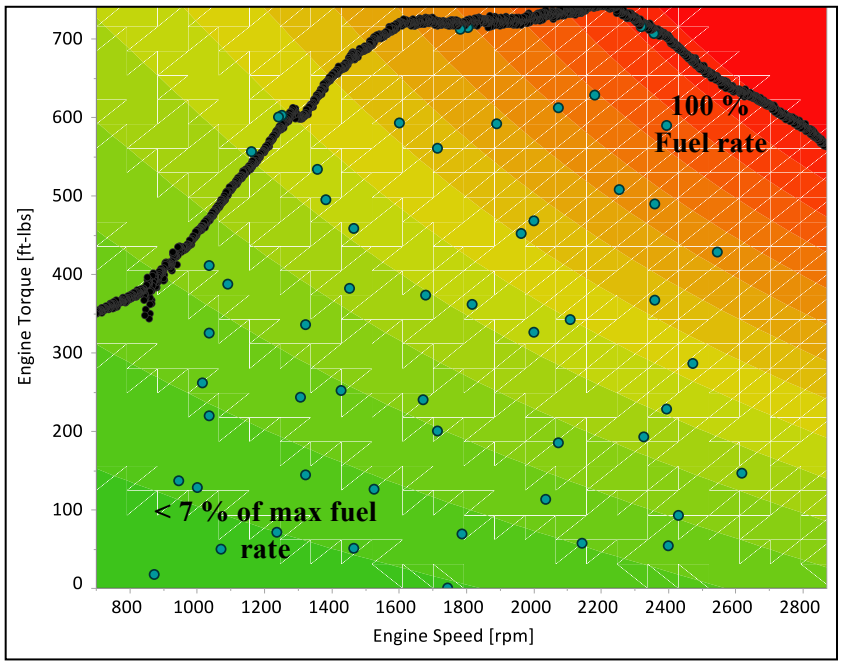

Figure 22. Contour plot prediction for Cummins ISB6.7 fuel flow rates [g/s]

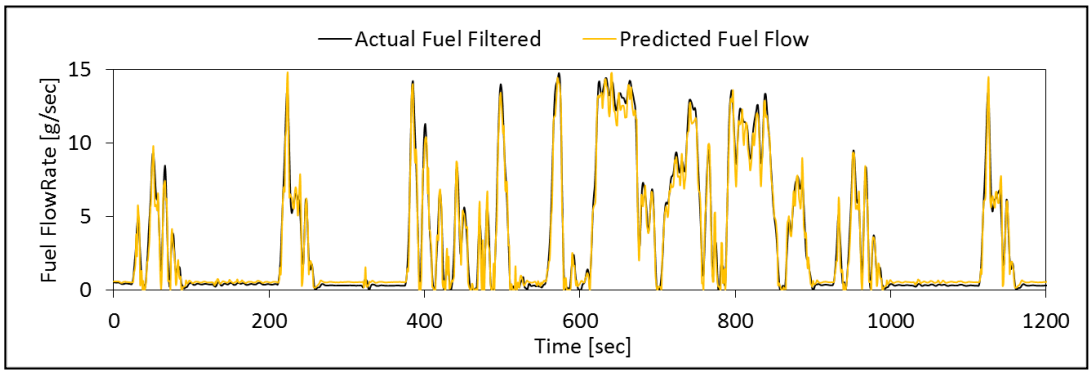

Figure 23 Comparison of predicted vs actual instantaneous fuel consumption over FTP

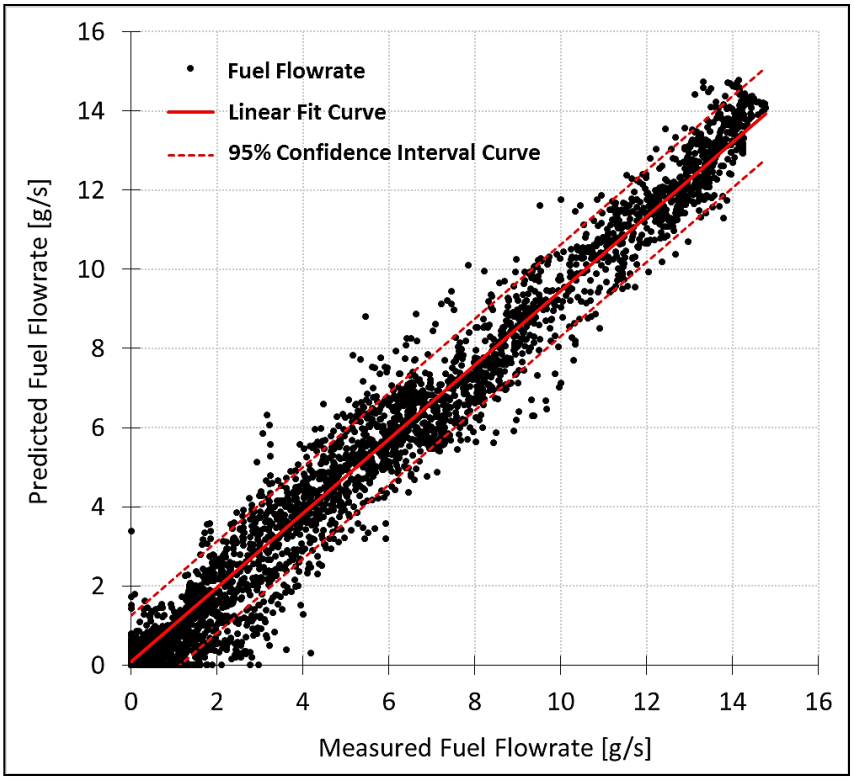

Figure 24 Scatter Plot predicted vs measured fuel flow for Cummins ISB over FTP

Table 11 Fit statistics for the predicted vs measured fuel consumption for Cummins ISB

Total FTP Cycle Fuel	
Actual Total Fuel [g]	4120.9
Predicted Total Fuel [g]	3980.5
Percentage error of integrated fuel	3.41%
Total FTP Work (kW-hr)	14.6
Summary of Linear Fit	
RSquare	0.978
Root Mean Square Error	0.604
Mean of Response	3.29
Number of Data Points	6045

Figure 24 shows the scatter plot of predicted fuel consumption against measured instantaneous fuel consumption for the Cummins ISB 6.7 over the transient FTP cycle. The predicted value of the Cummins was obtained by fitting a second order fit through fuel consumption data points obtained through steady-state testing. Statistics of the fit (Table 11) show an under-prediction of fuel consumption by 3.41% between steady-state fuel map and measured fuel consumption over the FTP. Therefore, a correction factor of 1.034 is to be applied to the predicted fuel consumption so as to match the measured FTP fuel consumption.

5.2 Autonomie Fuel Map

The 2nd order fit equation developed using the combined steady-state and transient dataset was used to populate the 25 X 25 Autonomie fuel consumption matrix. The major technological difference between the MY 2005 and MY 2010 engine is related to the aftertreatment package. The MY2005 Mercedes was

not equipped with aftertreatment system while the MY 2010 Mack was equipped with a DPF and SCR system. Further, in order to achieve the US EPA NOx emissions limit of 0.20 g/bhp-hr, it can be expected that the MY 2010 engine operates with a higher EGR rate than a MY 2005 engine certified at 2.4 g/bhp-hr NOx standard. The higher EGR fraction can relate to an increase in pumping losses since the VGT has to restrict the flow of exhaust in order to drive exhaust gas back to the cylinders. In addition, the presence of DPF increases the exhaust backpressure, which comes with a fuel penalty. Improvements in engine technologies, as well as the use of SCR technologies, have alleviated some of the fuel penalty incurred due to stringent emissions regulation. The brake-specific fuel consumption of the Mercedes over the FTP was calculated to be 17.4 g/bhp-hr, while that of the 2010 Mack was calculated to be 16.6 g/bhp-hr.

5.3 Energy Audit

The results in this section detail the energy flows in a heavy- and medium duty diesel engine. The results in this section represent only 5 of the 50 steady-state test points over which the energy audit was calculated. The location of the 5 test points for which the energy audit was calculated are shown in Figure 25. Figure 26 shows the location of the 5 energy points of the medium-duty engine under the lug curve. The points represented were chosen from different regions of the lug curve to show the changes in energy distribution with different operating set points. The engine friction component of the friction and pumping loss manifests itself as heat energy in both coolant and exhaust energy, therefore the fraction of frictional loss is subtracted from the exhaust energy fraction to avoid double counting of energy distribution.

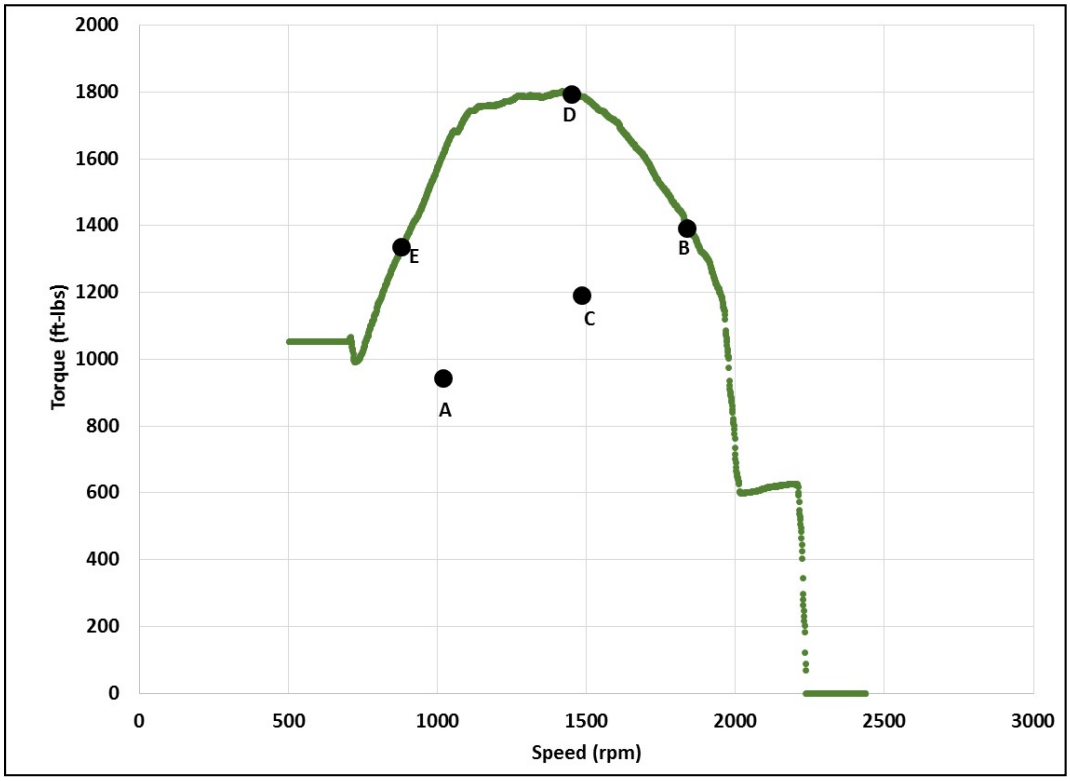

Figure 25 Location of 5 energy audit points under the lug curve of the heavy-duty diesel engine

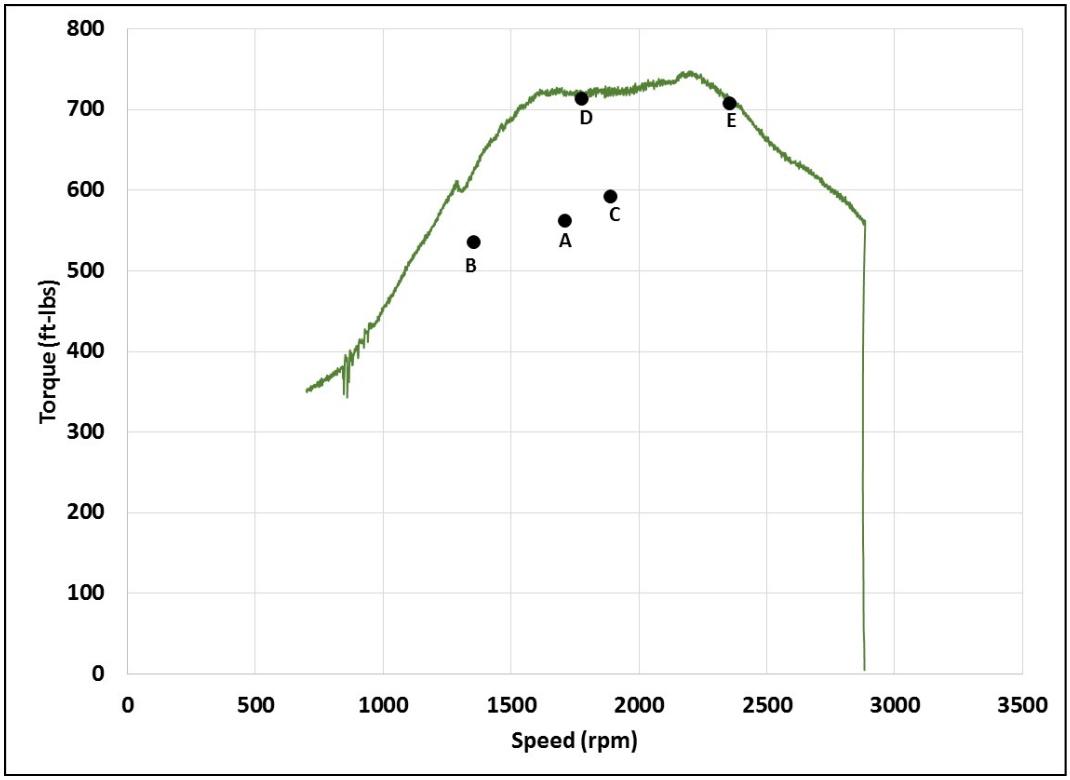

Figure 26 Location of 5 energy audit points under the lug curve of the medium-duty diesel engine

5.3.1 USEPA 2010 Heavy-Duty Engine Energy Audit

Figure 27 shows the results for energy distribution of the USEPA 2010 compliant heavy-duty diesel engine. The results of the energy audit show that on average 39% of the total input fuel energy is converted to useful work and an average 34% of the fuel energy is rejected as exhaust gas measured at the turbocharger exit. Frictional and pumping losses together account for about 6% of total input energy. The coolant circuit carries close to 10% of input fuel energy rejected from the combustion chamber, engine oil and EGR circuit. The EGR cooler energy is also transferred to the coolant and is part of the coolant heat rejection. Since the EGR is internally circulated within the control volume, it has not been represented as a separate energy flow in the results below. Assuming 100% heat transfer between EGR and coolant circuit, an average 46% of the coolant energy is contributed by the EGR circuit.

The total frictional and pumping losses derived from motoring tests were separated using operational curves for auxiliary devices and experimentally calculating engine backpressure losses as explained in Section 5.4.4 . Frictional losses due to bearings, piston and cylinder contact and lubrication oil viscosity accounted for about 2% of the total fuel energy and on average 47% of the total frictional and pumping loss of the engine. Pumping losses on average contributed to 2% of the input fuel energy and on average 29% of the total frictional and pumping losses.

The energy distribution and magnitude of losses in an engine vary over the different regions of the lug curve. The variation in losses and brake thermal efficiency (BTE) are closely related to changes in frictional power that is dependent on engine speed, in-cylinder pressure and lubrication. While the pumping loss is a function of EGR flow, soot accumulation in DPF, boost pressure and turbocharger efficiency.

The peak BTE for the heavy-duty platform was measured to be approximately 40%. The EPA certification data shows thermal efficiency at peak torque of 42.8%. It is to be noted that differences in BTE between OEM reported literature/certification data and this study can be due to differences in engine age, state of DPF loading and fuel properties. Since, the engine tested for this study was removed from a truck that had operated for over 250,000 miles; differences in BTE can be expected between new OEM products and in-use engine performance.

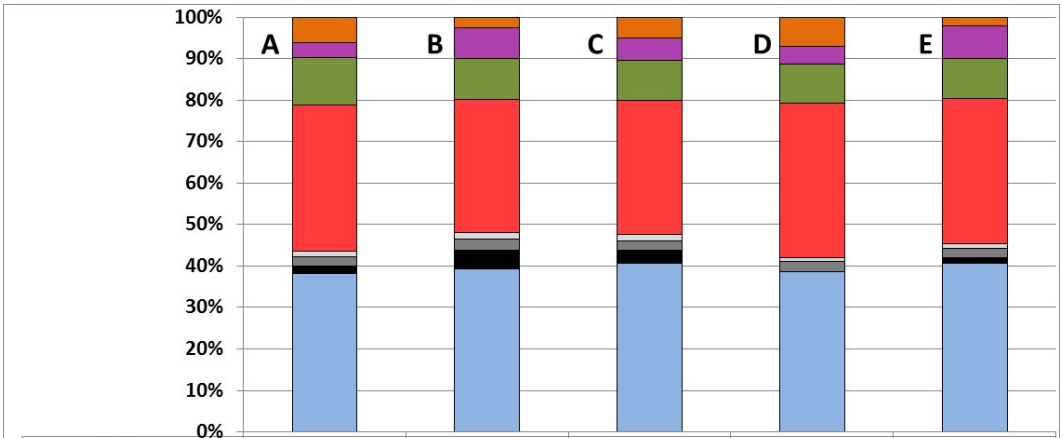

	A	B	C	D	E
Torque (ft-lbs)	943	1392	1192	1336	1793
Speed (RPM)	1019	1839	1486	881	1451
Fuel Energy	357.2	922.1	619.7	432.1	909.8
BTE	38%	39%	41%	39%	41%
Heat Transfer to Ambient	6%	3%	5%	7%	2%
Intercooler	3%	7%	6%	4%	8%
Coolant Energy	12%	10%	9%	9%	10%
Exhaust Energy	35%	32%	32%	37%	35%
Engine Auxiliaries	1.5%	1.6%	1.6%	1.0%	1.1%
Pumping Loss	2.2%	2.5%	2.2%	2.3%	2.3%
Engine Friction Loss	1.7%	4.5%	3.3%	0.1%	1.4%
Brake power	38%	39%	41%	39%	41%

Figure 27 USEPA 2010 heavy-duty energy audit for select operating points

5.3.2 USEPA 2010 Medium-Duty Engine Energy Audit

Figure 28 shows the results for energy distribution of the USEPA 2010 compliant medium-duty diesel engine. The results of the energy audit show that on average 40% of the fuel energy is converted to useful work while close to 36% of the energy is rejected as exhaust heat calculated at the turbocharger exit. Energy loss to engine friction accounts to an average 4.4% of fuel energy while energy loss to pumping and engine accessories accounts to an average 1.7% and 0.8% respectively. While on average, 9% of fuel energy is rejected through the coolant circuit. Assuming 100% heat transfer from the EGR to the coolant circuit, an average 49% of coolant energy is contributed by the EGR circuit. Peak BTE for the medium-duty diesel engine was calculated to be 41%.

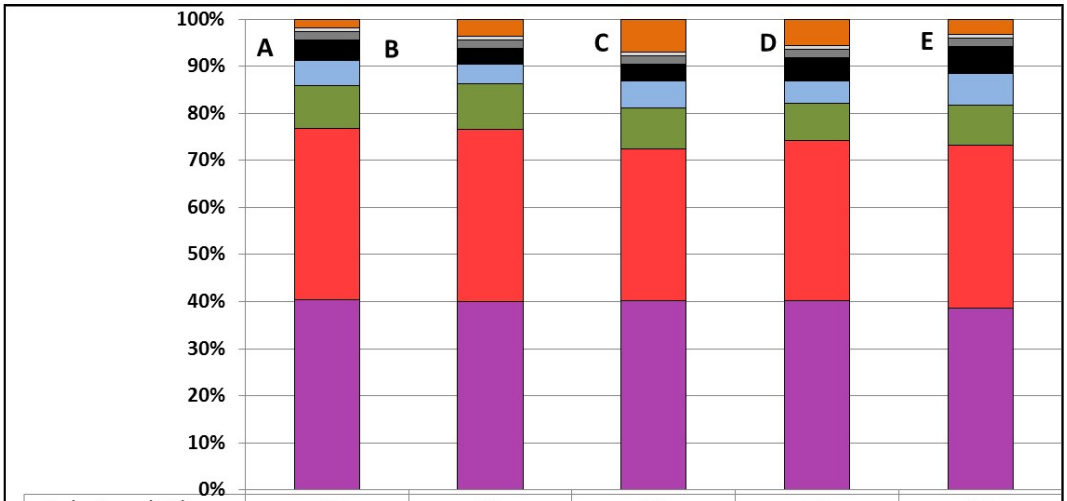

	A	B	C	D	E
Brake Power (KW)	137	103	180	159	237
Torque (ft-lbs)	561	534	712	591	707
Heat Transfer to Ambient	2%	4%	7%	6%	3%
Engine Auxiliaries	0.9%	0.9%	0.7%	0.9%	0.8%
Pumping Loss	1.7%	1.7%	1.7%	1.7%	1.7%
Engine Friction Loss	4.5%	3.3%	3.6%	5.0%	5.8%
Intercooler Power	5%	4%	6%	5%	7%
Coolant Energy	9%	10%	9%	8%	8%
Exhaust Energy	36%	36%	32%	34%	35%
Brake Power	40%	40%	40%	40%	39%

Figure 28 USEPA 2010 medium-duty engine energy audit for select operating points

5.4 Future Engine Prediction

The study developed fuel maps representative of future engines compliant to the 2017 and later US EPA GHG standard. We sought to estimate a reasonable technology configuration that is likely to be applied in a widespread manner for model year 2017 engines in the US. The study estimated loss reduction factors for the various loss mechnisms as a result of the improved engine technology configuration, in order to predict the future fuel consumption. The goal of the future engine fuel map prediction was to develop a fuel consumption profile that would satify the 460 g/bhp-hr CO_2 standard over the SET for heavy heavy-duty engine and a 576 g/bhp-hr CO_2 standard over the FTP for a medium heavy-duty engine (US EPA, 2011).

The US EPA rulemaking assesment provides the technology pathways for achieving the proposed 2017 GHG regulation for medium and heavy heavy-duty diesel engines. In this assessment, EPA and NHTSA project that the combination of incremental improvements in parasitic and friction losses via improved piston designs, lubrication, water pump and oil pump designs, lower differential pressure EGR system and better handling of air flow through the intake and exhaust systems would contribute to engine efficiency improvements to achieve the 2017 GHG compliance. In addition to parasitic losses, other engine design considerations will improve other loss mechanisms such as exhaust and coolant losses to reduce the fuel consumption further.

In order to scale the fuel consumption based on improvements to parasitic losses, water pump, oil pump and exhaust backpressure, it is necssary to separate the energy consumption categories individually. Since the measurement of friction and pumping losses together does not yield this categorical information, this study used literature, product specification and communications from OEMs to get speed-based power

consumption for water, oil and air compressor work. The frictional power obtained from motoring tests were split into its various components as follows:

5.4.1 Oil Pump

The oil pump work was derived from literature that details pump work from a 15 liter heavy-duty diesel engine (Lasecki and Cousineau, 2003). Figure 29 shows the linear curve of the oil pump derived from literature. The illustrated curve was used to calculate a speed based oil pump work for the 15 liter heavy-duty engine platform.

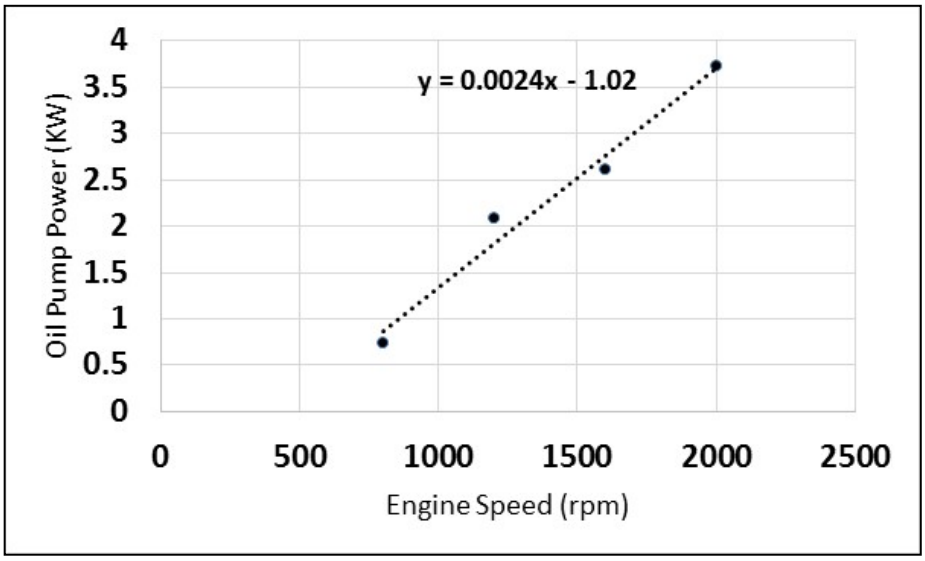

Figure 29 Oil pump power requirement vs engine speed (Lasecki and Cousineau, 2003)

5.4.2 Water Pump

The power requirements of heavy-duty engine water pumps were provided by OEM input based on an idle speed power requirement and rated speed power requirement. Hence, a 2-point linear relationship was used to calculate the speed-dependent water pump power requirement for the baseline 2010 heavy-duty diesel engine. Figure 30 shows a speed-based linear water pump curve derived from communication with an OEM.

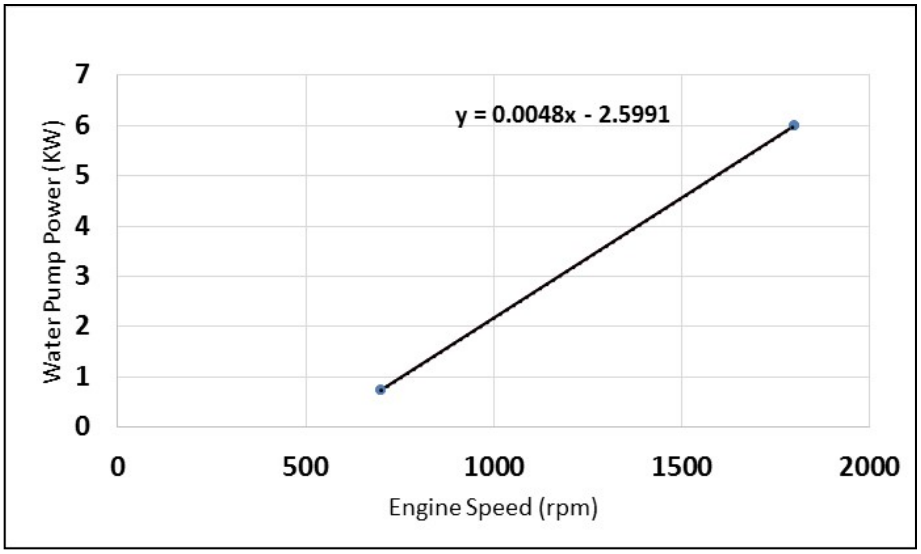

Figure 30 Water pump power requirement vs. engine speed

5.4.3 Air Compressor

Since the air compressor on-board the engine was disconnected during testing, only the unloaded air compressor friction component was calculated. Specifications provided by Cummins in a report for a 18.7 CFM WABCO air compressor were used to develop a linear relationship between engine speed and air compressor power requirements (Cummins, 2014b). Figure 31 illustrates the speed based power consumption of an air compressor in a heavy-duty diesel engine.

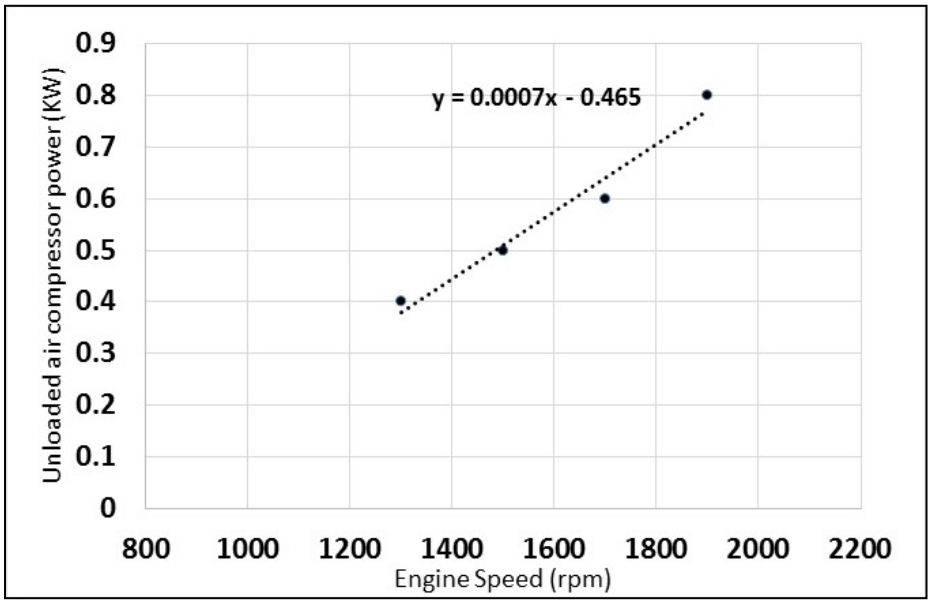

Figure 31 Unloaded air compressor power requirement vs engine speed (Cummins, 2014b)

5.4.4 Exhaust Backpressure

In order to separate the influence of exhaust backpressure on the pumping loss, The Volvo D13 engine was mapped at wide-open-throttle under different exhaust back pressure settings. The changes in total fuel consumption as a function of exhaust backpressure were determined to correlate mass of fuel

consumed to overcome a unit psig of backpressure. The results showed that 0.075 kg of fuel is used to overcome 1 psig increase in backpressure. In terms of fuel energy this translated to 3209.3 kJ of fuel needed to overcome 1 psig of exhaust backpressure. This simple relationship was used to scale the fuel energy as a function of percent reduction in exhaust backpressure.

5.4.5 Engine Friction

The afforementioned components were considered as the measurable fraction of friction and pumping. The remaining fraction of the total friction and pumping power was attributed directly to engine piston seals, connecting rod and crankshaft bearings, lubrication oil viscosity effects, and fuel pumps.

The summation of the afforementioned frictional and pumping components will equal the frictional fraction of input energy shown in the 2010 reference engine energy audit results.

5.4.6 Prediction Methodology

For the prediction of the 2017 and 2020 fuel maps, an extensive literature survey was conducted to identify areas of improvements suggested by OEMs and the resultant fractional improvement in fuel economy. These improvements were factored in as lower energy consumption by the respective components and an updated fractional energy summation is derived. This updated energy audit fraction will sum to less than 100% due to the reduction in energy consumption by various factors. Hence, the updated fuel energy will be calculated as the summation of the newly reduced energy distribution of the various fractions. For the 2020+ maps the WHR potential was factored as equivalent reduction in fuel energy for a specific speed and torque operating condition, without any effect on the loss category distribution. Since, the WHR potential is predicted to be a 2020+ technology, rather than a 2017 engine technology, the WHR simulation was not factored into the 2017 engine maps.

For the development of the 2017 and 2020+ maps, the different loss categories (friction, pumping, exhaust, etc.) were scaled down by a constant factor in order to estimate the incorporation of technology developments. Technology advancements reviewed to factor in the percent reductions for individual categories are discussed below.

5.4.6.1 Pumping Loss Improvements

The EGR circuit and exhaust aftertreatment backpressure can be considered as a major factor contributing to the baseline engine pumping loss. It can be projected that with improvements to low temperature operation of SCR catalysts and partial hybridization of thermal management strategy, can effectively contribute to lower EGR mass fractions, therefore, reducing the demand for higher exhaust manifold pressure to drive the EGR flow to the intake manifold. This reduction in EGR demand can significantly reduce the parasitic pumping work of the engine.

Daimler has shown that through the use of their patented asymmetric turbocharger with no moving vane actuation, smaller and lighter components than traditional VGT, is able to achieve both superior air delivery performance and up to 35% EGR rates at full load on the Detroit Diesel's heavy-duty platform. This highly efficient design utilizes a group of cylinders as a dedicated EGR pump while another set of cylinders is dedicated for turbocharging purposes (Chebli et al., 2013). Technology improvements in turbomachinery can contribute to greater than 5% improvement in fuel consumption. Grouping of exhaust manifolds based on firing order provides an efficient turbocharging process with lower pumping loss fraction to drive EGR fractions of up to 35% (Chebli et al., 2013).

Another contributor to engine backpressure is the DPF. Research from Corning Inc. has shown the possibility of thin walled DPF substrates to lower exhaust backpressure by approximately 35% (Corning).

Overall, this study assumes that changes in exhaust and air handling components of the engine can lower pumping losses by close to 30%.

5.4.6.2 Engine Accessories

Variable flow oil pumps and coolant pumps can contribute up to 2% reduction in fuel consumption for heavy-duty applications (Concentric, 2014). A model year 2013 Detroit diesel DD15 engine uses a viscous clutch design to improve water pump efficiency compared to traditional gear driven pumps (Daimler, 2014). Decoupling of oil and water pump at lower engine loads help reduce pump friction during closed thermostat engine operation. This could be a potential design feature for future engines beyond 2017, to use oil and water pump decoupling when not required for engine cooling purposes.

Electric oil pumps that can be varied based on engine load conditions and oil temperature have shown to reduce parasitic and frictional losses during cold start and low load operation. However, there are cross-interactions with alternator loading that must be balanced efficiently to acquire an overall benefit. Overall, this study assumes that engine accessories power consumption can be reduced by about 10% in future engines.

5.4.6.3 Engine Friction

A study by Fenske et al. has shown that the combination of bearing and piston coating materials and introducution of low-friction boundary lubrication technologes can reduce fuel energy consumed by friction by about 5% (Fenske et al., 2014). Synthetic lubrication oils and advanced oil formulation can significantly reduce engine friction. Cummins showed a 30% reduction in friction from a MY 2009 ISX by use of reduced-friction shafts seal, variable flow oil pump, optimized water anf fuel pump, reduced friction in gear train and cylinder piston friction components (Delgado and Lutsey, 2014). A study by Grant showed that a low-friction piston ring design can contribute to 30-35% reduction in engine friction resulting in a 0.5% to 1% improvement in BTE (Grant, 2004). This study assumes that engine friction can be reduced by 25% in future engines.

5.4.6.4 Exhaust Energy

Improvements to turbomachinery and to combustion parameters such as increased compression ratio and increased peak in-cylinder pressures will contribute to the largest fuel savings within this loss category. Efficient use of exhaust energy in the turbine stage of advanced turbocharger designs will provide increased power density to the engine with efficient air and EGR delivery to the intake manifolds. Turbo designs such as the asymmetric turbocharger from Daimler has shown significant improvement in turbocharging performance over the widely used VGT based turbocharger (Chebli et al., 2013). Improving the turbine efficiency of the turbocharger will directly contribute to lower exhaust energy through efficient conversion of exhaust energy to deliver high-pressure ratio in the compressor side of the turbocharger. A future two-stage turbocharging concept developed by Cummins features patented exhaust flow control that helps optimize the turbine operation. The two-stage turbocharging concept is aimed at delivering ultra-high boost, higher power density and deliver 1 to 2 percent fuel consumption benefit (Cummins, 2014a, Cooper et al., 2009). NRC reports that turbocharging concepts can deliver a 2-5 percent reduction in fuel consumption while providing the required EGR flow (NRC, 2010). This study projects a 10.5% reduction in fuel consumption through exhaust energy reduction for the 2017 engine technology. Of which, this study projects the turbocharging technology to contribute to close to 15% reduction in exhaust energy, therefore, resulting in a 5% reduction in fuel consumption. Mechanical or electrical turbo-compounding technology can further utilize exhaust energy downstream of primary turbocharger to develop useful mechanical work delivered to flywheel or electrical work for charging batteries and powering auxiliary system. Factoring in the effect of turbo-compounding in a simple

thermodynamic assessment of engine loss reduction is difficult. Therefore, the study assumed the impact of turbo-compounding as an exhaust energy loss reduction mechanism that contributes to fuel savings. Callahan et al. show that the mechanical turbo-compounding concept in the Detroit Diesel DD15 platform can contribute up to 2.5% reduction in fuel consumption at full load operating conditions. This reduction also factored in the pumping loss encountered due to an additional work producing turbine in the exhaust pathway (Calllahan et al., 2012). Further improvements to the turbo-compounding concept can be expected in the 2020+ period, with maximum projected fuel consumption benefits of up to 3.5% possible through this pathway (Cooper et al., 2009). Therefore, this study projects the 2020+ platform to benefit from an additional 3.5% reduction in fuel consumption..

Efficient conversion of combustion energy to work is another pathway to reducing fuel consumption. Thermally efficient engines with improved in-cylinder work extraction will invariably result in lower exhaust energy. Improvements to combustion chamber design and in-cylinder charge motion distributes the combustion energy evenly in the combustion chamber. The even distribution of in-cylinder energy will improve the expansion work of the piston. Improved fuel atomization through increased fuel injection pressures can achieve a uniform in-cylinder fuel/air ratio and thereby promoting greater conversion of fuel energy to work. Therefore, a better utilization of combustion energy to produce expansion work will result in lower total heat carried by the exhaust gases from the cylinder. A study conducted by Southwest Research Institute (SWRI) show that a combination of two-step piston design and 8-nozzle fuel injector can provide close 5% lower brake-specific fuel consumption (BSFC) compared to conventional piston design with a 6 nozzle injector geometry (Roberts et al., 2011). The improved piston geometry and larger number of injector nozzles creates faster burn rates and high cycle efficiency. However, this study demonstrated these benefits only at medium speeds and high load condition. The average improvement on BSFC throughout the lug curve will be lower than the 5% BSFC reduction shown in this study (Roberts et al., 2011). By assuming a 3% reduction in fuel consumption through a combination of improved cylinder geometry, injector design and higher injection pressures, this study projects an additional 8.5% reduction in exhaust energy compared to the baseline 2010 engine platform. Navistar achieved 3% absolute improvement in BTE using higher compression ratio, higher peak cylinder pressures (220 bar) and high-pressure common rail system capable of fuel pressures in the range of 2900 bar (Delgado and Lutsey, 2014). A 3% absolute increase in BTE corresponds to an average 8% reduction in fuel consumption. Since many of the combustion improvements increase cycle efficiency, a lowering of exhaust energy is expected. And the 8.5% reduction in fuel consumption projected by Navistar, relates to a 25% reduction in exhaust energy fraction through the analysis shown in this study. Cummins showed a 2% absolute improvement in BTE through engine design improvements that include compression ratio, piston bowl shape and engine calibrations (Delgado and Lutsey, 2014). It is to be noted that the BTE figures provided from the Super Truck project may be representative of fuel consumption benefits incurred only at a specific region of the lug curve, while this study assumes a uniform reduction in loses throughout the lug curve.

Advancing injection timing has shown to improve engine efficiency, lower BSFC, and lower exhaust temperature. However, a possible increase in NOx emission is a disadvantage of advancing injection timing. Advancement in NOx aftertreatment technology is imperative to realize the benefits of advancing injection timing. OEMs can implement engine calibration with advanced injection timing only with suitable aftertreatment concepts that offer higher NOx reductions at lower exhaust temperatures. Ardanese et al. developed a low fuel consumption engine calibration map that utilized an optimized urea dosing strategy as an approach for meeting US EPA 2010 emissions standards while achieving a low fuel consumption (Ardanese, 2008). This low fuel consumption calibration characterized by advanced injection timing resulted in a 4% decrease in exhaust temperatures (Ardanese, 2008). A presentation by

Stanton shows a similar finding where an advanced SCR aftertreatment system has contributed to 10% reduction in fuel consumption while increasing the engine out NOx by eight fold. (Stanton, 2009). The study concluded that such a strategy complemented with an advanced NOx reduction aftertreatment strategy could help utilize the fuel consumption benefit of advancing injection timing. Closed loop controls such as in-cylinder combustion feedback and optimized fueling strategy through neural network strategies can lead to further reductions in fuel consumption and consequently a lower exhaust energy profile from future 2020+ engine technologies (NRC, 2010). Real-time combustion control, advanced fuel injection concepts, and alternative combustion strategies can contribute to an additional 1 to 4 percent reduction in fuel consumption (NRC, 2014). Since, such reduction directly influence the close cycle efficiency of the engine, lower heat rejection through exhaust gases can be expected. Therefore, this study identifies that a maximum of 4% reduction in fuel consumption translates to a 10% reduction in exhaust energy from the baseline engine energy audit.

This study projects a 15% reduction in exhaust energy for the 2017 engine platform, and an additional 25% reduction for the 2020 engine technology. The on-going research cited in this discussion shows that adequate technology pathways have been identified previously that justify the reduction targets used in this study.

5.4.6.5 Coolant Energy

Lowering engine friction and reduction in EGR fractions will result in lower heat carried by the coolant circuit. Future engines could be characterized by reduced EGR rates owing to improved NOx aftertreatment systems. Integrated DPF and SCR aftertreatment systems can help improve low temperature catalyst activity and as a result help towards cutback of EGR fractions used for in-cylinder NOx reduction. Reduced EGR can help reduce both pumping loss as well as heat rejected into the coolant circuit from the EGR cooler.

Better utilization of combustion energy for expansion work will also cause reduction in heat rejected to coolant from combustion chamber. Reducing heat transfer from combustion chamber will increase available energy for expansion work. Stanton shows that improvements to materials technology, insulation of combustion chamber, lower friction components and reduced EGR fraction can reduce heat loss through coolant circuit and improve fuel consumption by close to 3% (Stanton, 2013). Reduced heat transfer from combustion chamber to coolant circuit will significantly improve the thermal efficiency. Based on the energy distribution assessed in this study, a 3% reduction in fuel consumption from coolant energy reduction translates to a 30% reduction in coolant energy losses. This study projects a 1.6% reduction in fuel consumption obtained through a 15% reduction in coolant energy for the 2017 platform, while a 2.2% reduction in fuel consumption with a 25% reduction in coolant heat loss is projected for 2020+ engine technology.

Table 12 shows the contribution of the different technologies to the various energy audit categories as well as forecasting availability of the various improvements.

Table 12 Efficiency technologies, energy loss mechanism they influence, and approximate timeframe of technology availability

Engine technology that offers potential efficiency improvement over representative model year 2010 technology	Engine loss areas where the technology reduces the energy loss[a]					Technology available before 2020	Technology available in 2020 -2030
	Heat loss engine coolant system	Heat loss exhaust system	Engine pumping (intake, exhaust)	Engine friction losses	Auxiliary/ accessory		
Compression ratio increase		X				X	X
Feedback engine controls	X	X			X		X
EGR improvements			X			X	X
Low friction lubricants				X		X	X
Engine friction reduction				X	X	X	X
Parasitic load reduction (piston)				X		X	X
Parasitic load reduction (water)				X		X	X
Parasitic load reduction (fuel pump)				X		X	X
Parasitic load reduction (oil pump)				X		X	X
Turbocharging and other air handling system improvements		X	X			X	X
Fuel injection improvements (e.g., increased fuel rail pressure)		X				X	X
Optimized cylinder head design		X				X	X
Aftertreatment improvements and optimization		X	X			X	X
Advanced waste heat recovery systems					X		X
Turbocompounding		X				X	X

[a] *Technologies (left) that impact each energy loss mechanism (top) marked with "X"*

The prediction methodology adopted in this study was aimed at providing a holistic view of the expected fuel consumption benefits that can be obtained from the engine technology advancement pathways identified by industry researches. It is important to understand that some technology pathways will have negative cross-interactions that might undermine the total magnitude of benefits that could be obtained. Factoring in such cross-interactions is beyond the scope of the study and hence not factored. Further, the fuel consumption benefits shown in this study, subject to the challenges of satisfying future emissions regulations, and engine durability criteria that OEMs will be faced with. This study uses a simple energy balance principle to predict future fuel maps based on categorically reducing losses by a certain factor. The reductions are aimed at developing a fuel map for a heavy- and medium-duty engine compliant to the 2017 USEPA GHG standard. Therefore, the actual magnitudes of the energy distribution of the future engines, could be different from the results shown in this study. However, it is expected that the fuel consumption characteristics projected in this study will be representative of future engines.

5.4.7 2017 Engine Map Analysis

Table 13 shows the list of engine improvements considered and the percent reduction in fuel energy reviewed from literature for the 2017 engine technology. The table lists the major factors considered for predicting the 2017 equivalent engine technology's fuel consumption.

Table 13 List of engine improvements considered for developing 2017 heavy-duty engine maps for SET prediction

Category of energy loss	% Fuel in loss mechanism	% Reduction in Loss Mechanism	% Fuel Savings
Exhaust Energy	35.52	15	5.33
Coolant	10.68	15	1.60
Friction	2.32	15	0.35
Pumping	1.7	30	0.51
Engine Accessories	1.3	10	0.13
Ambient Heat Transfer	4.3	0	0
		Total	7.92

Figure 32 shows the projected frictional torque of the 2017 engine technology. The figure illustrates the difference in the baseline frictional torque measured through motoring experiments, and the projected frictional torque obtained by lowering the friction and pumping losses with improved engine technology. The lower friction and pumping loss results on an average 14% lower frictional torque compared to baseline engine technology. Improving the EGR circuit to account for lower pumping loss and improvements to aftertreatment technology contributed to the majority of the fuel savings in the friction and pumping loss category.

Fuel pump in an engine is an important accessory device that consumes up to 2% of input fuel. In this study, the fuel pump contribution is accounted for in the engine friction loss category. With a lack of accurate fuel pump characteristics and actual engine injection pressure, however, it is difficult to model the load-based power consumption of the fuel pump. Combustion improvement pathways such as increased fuel rail pressure will have negative cross interaction with higher power consumption from the fuel pump. Such interactions were neglected in this study, since design and operation of modern fuel pumps are proprietary and therefore not available.

Table 14 Comparison of SET fuel consumption and brake specific-CO_2 between baseline 2010 and projected 2017 heavy-duty diesel engine

	Baseline 2010	Projected 2017
SET Work (bhp-hr)	118	118
Total Fuel (kg)	18.9	17.4
CO_2 (g/bhp-hr)	498	459
** Fuel to CO2 conversion factor of 3106 g of CO2 per Kg of diesel Fuel with SG of 0.849* ** Baseline EPA/NHTSA brake-specific CO2 for HD diesel set as 490 g/bhp-hr*		

Table 14 shows the total fuel consumed over the SET cycle for the tested baseline 2010 heavy-duty engine and the projected fuel consumption of the 2017 engine platform. The 7.9% fuel consumption reduction projected in this study is as a result of factoring in reduction from a baseline brake specific-CO_2 of 498.3 g/bhp-hr as opposed to the 490 g/bhp-hr provided in the EPA and NHTSA rule making. The conversion factor of mass of fuel to mass of CO_2 was calculated using WVU engine lab test results of fuel consumed and CO_2 measured. A value of 3106 g of CO_2/ Kg of fuel was calculated and used for calculation of brake specific-CO_2 emissions from baseline and projected engines. The baseline CO_2 emissions are an approximation based on the mass of fuel consumed and not a result of emissions measurement. The fuel consumption reduction for the 2017 engine was factored to achieve at a minimum the 2017 CO2 standard of 460 g/bhp-hr.

Since, the baseline brake specific-CO_2 in this study is 1.7% higher than the baseline set forth by EPA and NHTSA, the reductions calculated to achieve 2017 compliance, in this study, is as a result, higher than the expected reduction of 6.5% projected by the EPA and NHTSA (USEPA, 2011). It must be noted that, upon emissions testing the baseline 2010 engine tested in this study emitted 492 g/bhp-hr CO_2 (See Appendix) over the SET cycle. Since, this study was initially proposed to be conducted without any emissions measurements, the results of emissions testing was simply used to verify the EPA baseline brake specific-CO_2.

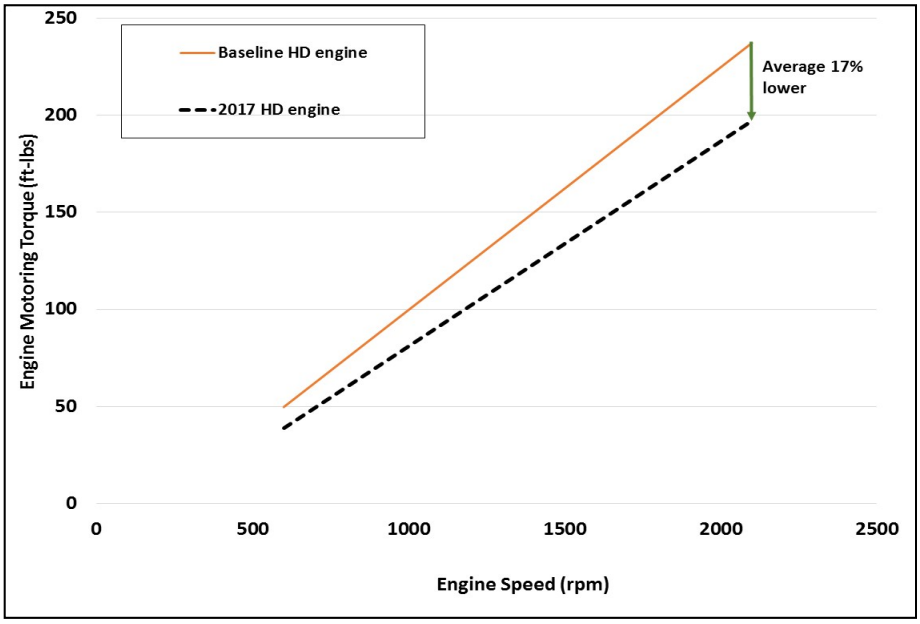

Figure 32 Projected 2017 engine frictional torque

Figure 33 shows the baseline heavy-duty engine map with percent difference in fuel consumption between baseline fuel consumption rate and the reduced fuel consumption predicted for 2017 engine technology. A 7.9% reduction in fuel consumption was predicted over the SET cycle using the 2017 fuel maps.

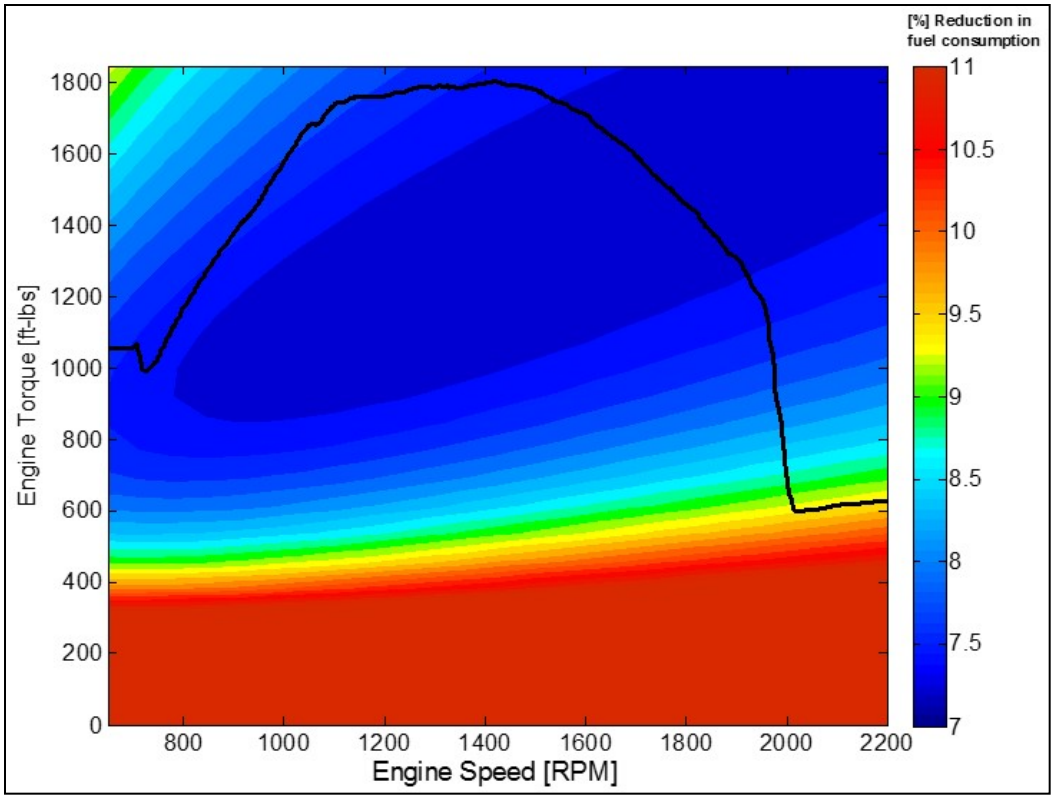

Figure 33. Reference engine map, with percent fuel consumption reduction for the estimated 2017 engine technology

Figure 34 shows the projected BTE for the 2017 engine technology calculated using the 2017 engine fuel maps. A maximum BTE of 44% is projected between 50% to full load at engine speeds between 1200 to 1800 rpm. The projected BTE is consistent with engine downspeeding strategies that would involve the operation of an engine at consistent lower speeds using intelligent transmission concepts.

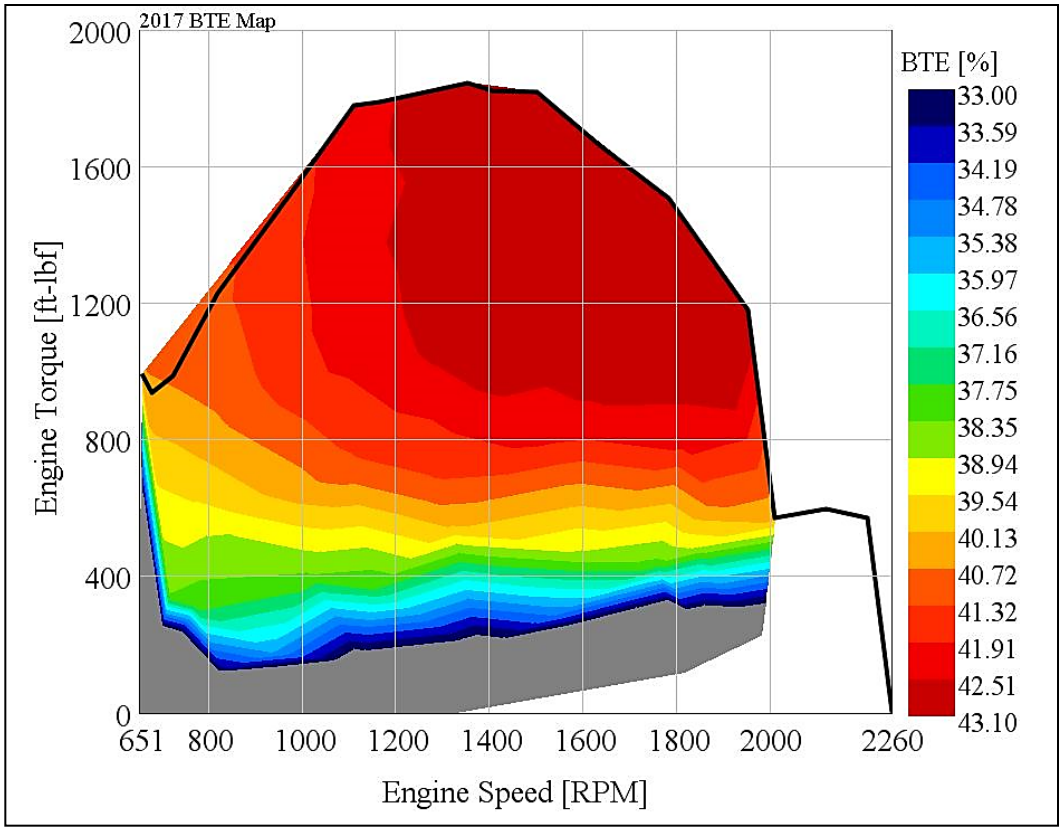

Figure 34 Predicted BTE for 2017 engine technology over the lug curve

5.4.8 2020+ Engine Map Analysis

The study further predicted the fuel consumption of future 2020+ engine technology using a similar approach to develop the 2017 engine fuel maps. This predicition utilized technology pathways consdidered for the 2017 prediction, while further extrapolating the benefits to achieve a maximum feasible reduction in loss mechanisms. The actual magnitude of benefits in future engines could be significantly different and would be dependent on regulatory standards and individual OEM technology pathways.

Table 15 shows the list of technolgies percent reduction in losses from the 2010 reference engine. The 2020+ fuel consumption prediction also included the use of a simulated WHR system to generate brake work. It is to be noted that the WHR system simulated in this study is based on the energy audit of the reference 2010 engine. Therefore, interlinking of the WHR simulation with the modified map of 2020+ is not straightforward as the WHR cycle efficiency is dependent on energy carried by EGR and coolant streams. Hence, the impact of WHR on the 2020+ energy distribution is reflected as a higher BTE provided by the additional WHR work for the same amount of fueling for the respective speed and torque points.

Table 15 List of Engine Improvements Considered for Developing 2020+ Heavy-Duty Engine Maps for SET prediction

Category of energy loss	% Fuel in loss mechanism	% Reduction in Loss Mechanism	% Fuel Savings
Exhaust Energy	35.52	40	14.21
Coolant	10.68	25	2.67
Friction	2.32	25	0.58
Pumping	1.7	40	0.68
Engine Accessories	1.3	10	0.13
Ambient Heat Transfer	4.3	0	0
		Total	18.27
Waste Heat Recovery			3.27
		Total	21.54

The 2020+ simulations without WHR showed an average 18.3.% reduction in fuel consumption over the SET cycle in comparison to baseline 2010 heavy-duty engine. The WHR system simulated in this study contributes to an additional 3.27% reduction to the baseline fuel consumption.

Table 16 Comparison of SET fuel consumption and brake specific-CO_2 between baseline 2010 and projected 2020+ heavy-duty diesel engine

	Baseline 2010	Projected 2020+	Projected 2020+ with WHR
SET Work (bhp-hr)	118	118	118
Total Fuel (kg)	18.9	15.4	14.7
CO_2 (g/bhp-hr)	498	431.3	409
** Fuel to CO2 conversion factor of 3106 g of CO_2 per Kg of diesel Fuel with SG of 0.849* ** Baseline EPA/NHTSA brake-specific CO_2 for HD diesel set as 490 g/bhp-hr*			

Table 16 shows the projected fuel consumption over the SET for the 2020+ engine technology with and without WHR system. The brake specific-CO_2 emissions for the 2020+ engine technology with and without WHR system was projected to be 431.3 and 408.9 g/bhp-hr respectively.

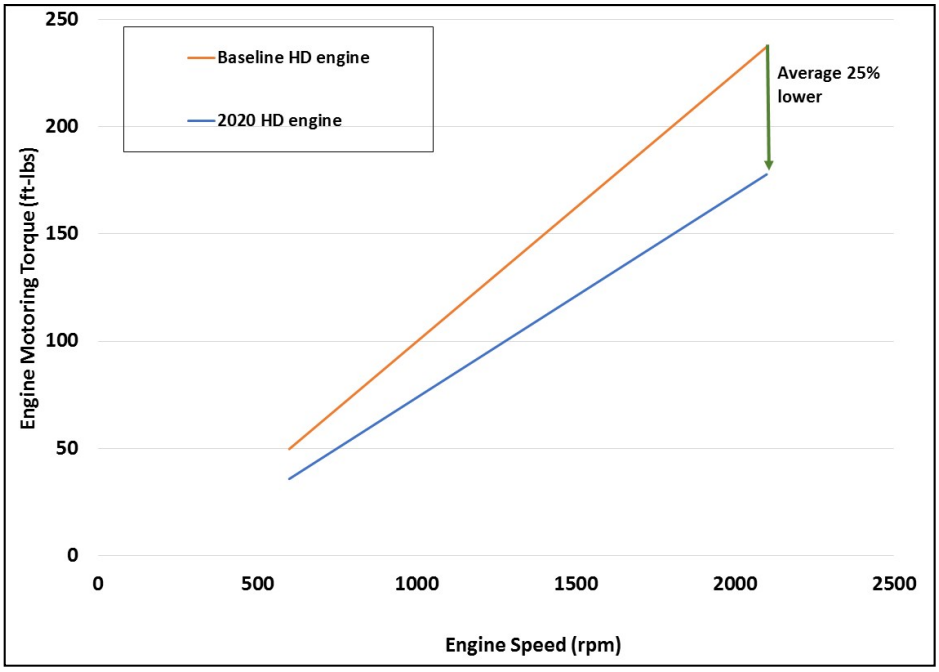

Figure 35 Projected 2020+ engine frictional torque

Figure 35 shows the predicted frictional torque curve for the 2020+ engine technology. The prediction shows an average 25% lower frictional torque as discussed above.

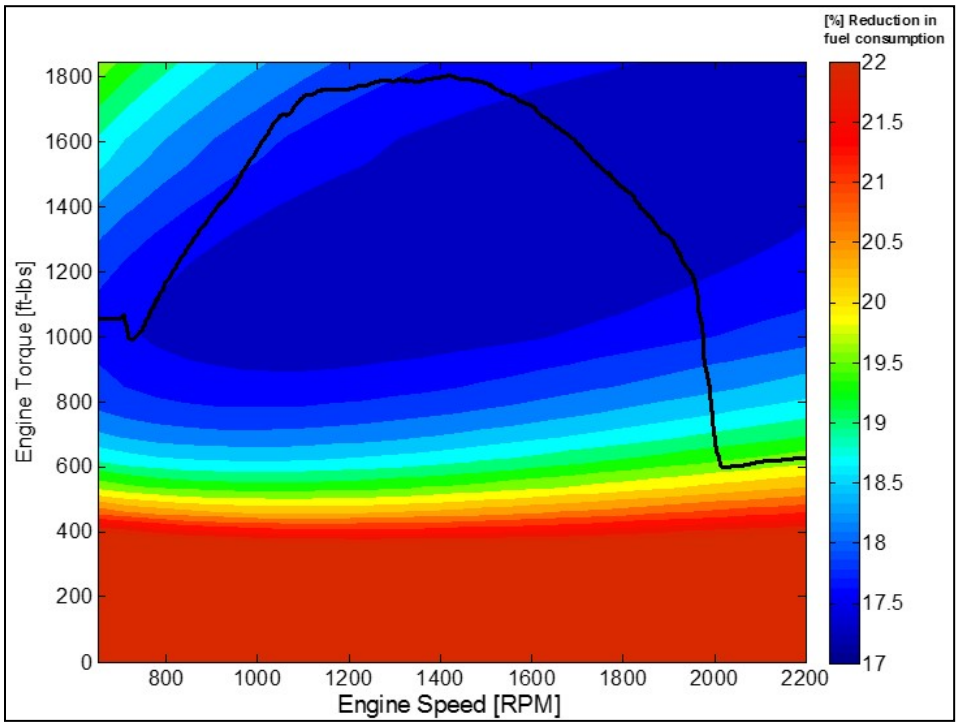

Figure 36 Engine map, with percent potential fuel consumption reduction for 2020+ efficiency technology compared to reference 2010 engine

Figure 37 shows the predicted BTE for the 2020+ engine technology. The results project a maximum BTE of 49% for the simulated 2020+ engine technology without WHR. The peak BTE points are observed between 40% and full load at engine speed between 1100 and 1800 rpm.

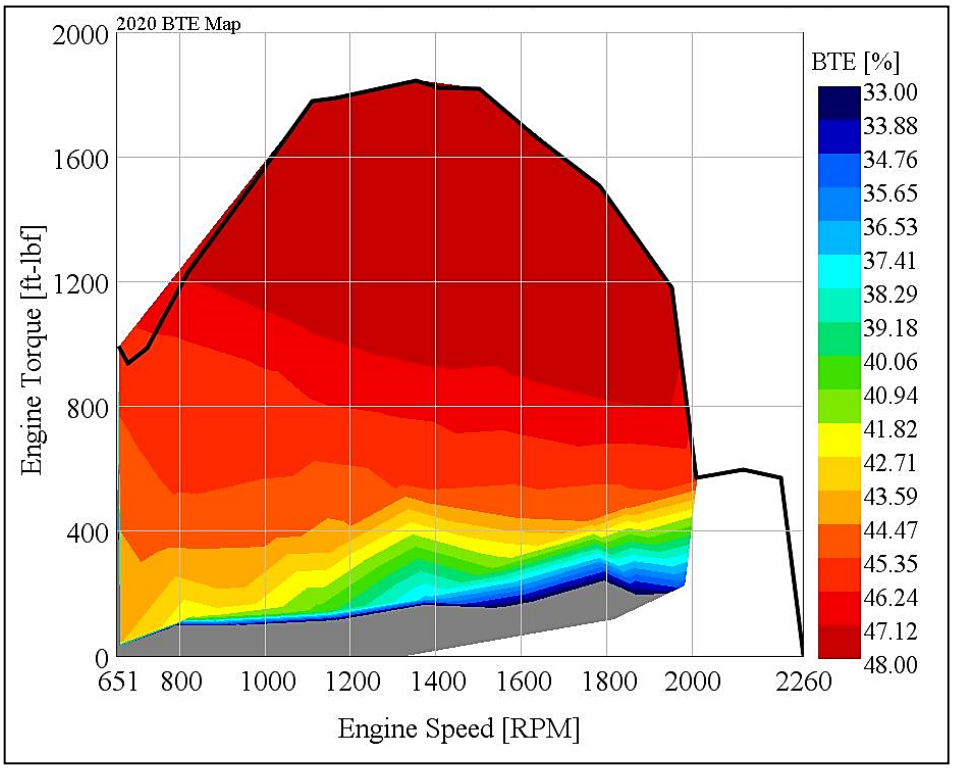

Figure 37 Predicted BTE for 2020+ engine technology over the lug curve

5.5 Regulatory Cycle Predictions

The energy distribution predictions for the 2017 and 2020+ engine technology were used to create maps of individual loss mechanisms that would represent 2017 and 2020+ engine technology. These maps were then used to predict the energy distribution over the SET for heavy-duty engine, and FTP for the medium-duty engine. The goal of the 2017 heavy- and medium-duty engine was to achieve the regulatory standard of 460 g/bhp-hr and 575 g/bhp-hr CO_2 respectively.

In the final rulemaking to establish the GHG emissions standards, the USEPA and NHTSA established baseline CO_2 emissions over the regulatory cycles of SET and FTP for heavy heavy-duty and medium heavy-duty engines respectively. Table 17 lists baseline brake-specific CO_2 emissions for a representative USEPA 2010 emissions compliant medium- and heavy-duty diesel engine (USEPA, 2011). EPA considered data from non-GHG certification applications, OEM data and tests conducted in US EPA laboratories to establish the below baseline performance.

Table 17 Baseline brake-specific CO_2 emissions established for USEPA 2010 emissions compliant medium and heavy heavy-duty engines (USEPA, 2011)

Medium Heavy-duty (FTP)	Heavy Heavy-Duty (FTP)	Heavy Heavy-Duty (SET)
630 g/bhp-hr	584 g/bhp-hr	490 g/bhp-hr

During this study, WVU observed baseline fueling of both the heavy-duty (See Appendix Table A1) and medium-duty engine (See Appendix Table A2) to differ from the US EPA established 2010 baseline values. The differences in the heavy-duty engine fuel consumption between certification data and WVU test data can be attributed to the age of the engine, state of DPF, operational conditions of engine components such as EGR coolers, fuel injectors, turbocharger and intake manifold. Engine losses can increase with age and can result in changes to fuel consumption compared to performance data provided by OEMs. Similarly, differences in the aftertreatment (DPF) state between OEMs performance condition and WVU test conditions could contribute to differences in fuel consumption. As a result the baseline fuel consumption during WVU testing, at peak torque is higher by 9% for heavy-duty platform and 7% for medium-duty platform compared to the fueling rate obtained from the EPA certification website (USEPA)). The higher fuel consumption obtained from WVU testing translates in to a higher fuel consumption reduction projected through this study compared to the projections in the USEPA rulemaking document to achieve 2017 SET standards (USEPA, 2011).

The study by Stanton shows a similar trend in fuel consumption reduction as simulated in this study (Stanton, 2013). WHR potential was marginally different between the estimations presented by Stanton and the results obtained from this study. Stanton's study indicates over 5% reduction in fuel consumption using WHR, while this study predicts 4% reduction in fuel consumption using WHR. It must be noted, however, that the 4% reduction is averaged over multiple points under the lug curve, and not the peak reduction in fueling obtained. Stanton's work serves as a good benchmark to compare the predictions obtained from this study to realistic pathways projected by the OEM.

Improvements in engine technology will invariably contribute to reductions in losses from a broad category of energy distribution mainly: exhaust energy, friction and pumping losses, and coolant energy. Of which exhaust energy is the major fraction of the energy loss categories. The study considered major reduction in exhaust and coolant energy for factoring in fuel consumption reductions. Industry research results that support this study's reduction percentages are explained in section 5.4.6.4. The 2020+ engine projection projects the maximum feasible benefits possible from all identified technology pathways. The regulatory predictions for 2017 and 2020+ were performed for both the heavy-duty and medium duty platform over the SET and FTP respectively.

5.5.1 Heavy-duty SET Prediction

Figure 38 shows the energy distribution for the reference 2010 and the predicted 2017 and 2020+ heavy-duty engine technology over the SET cycle. The predictions of the 2017 engine technology showed a 13.3% reduction in fuel consumption compared to the reference 2010 heavy-duty engine. The 2020+ engine technology represented maximum feasible fuel consumption reduction with further improvements to engine technology. The prediction resulted in a 17.8% reduction in fuel consumption over the SET compared to the reference 2010 heavy-duty engine.

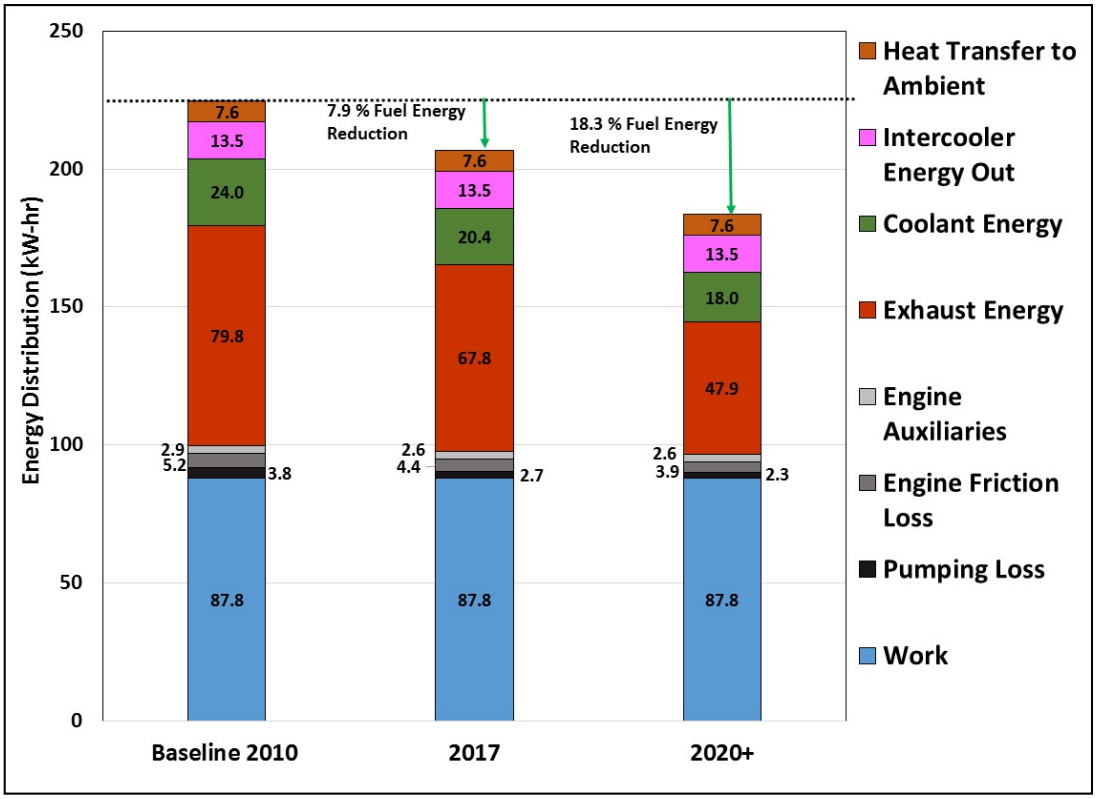

Figure 38 Heavy-duty energy loss distribution for 2010, 2017 and 2020+ engine technologies over SET

5.5.2 Medium-duty FTP Prediction

Figure 39 shows the energy distribution for the reference 2013, 2017 and 2020+ medium-duty engine over the regulatory FTP cycle. The projected fuel consumption reduction for the 2017 engine technology was calculated to be 10.6% while the maximum feasible fuel consumption reduction for the 2020+ engine technology was projected to be 19.5%. The reductions in ambient heat transfer shown in the figure is a result of error in the prediction of energy distribution on a transient FTP cycle and not a factored reduction in ambient heat transfer.

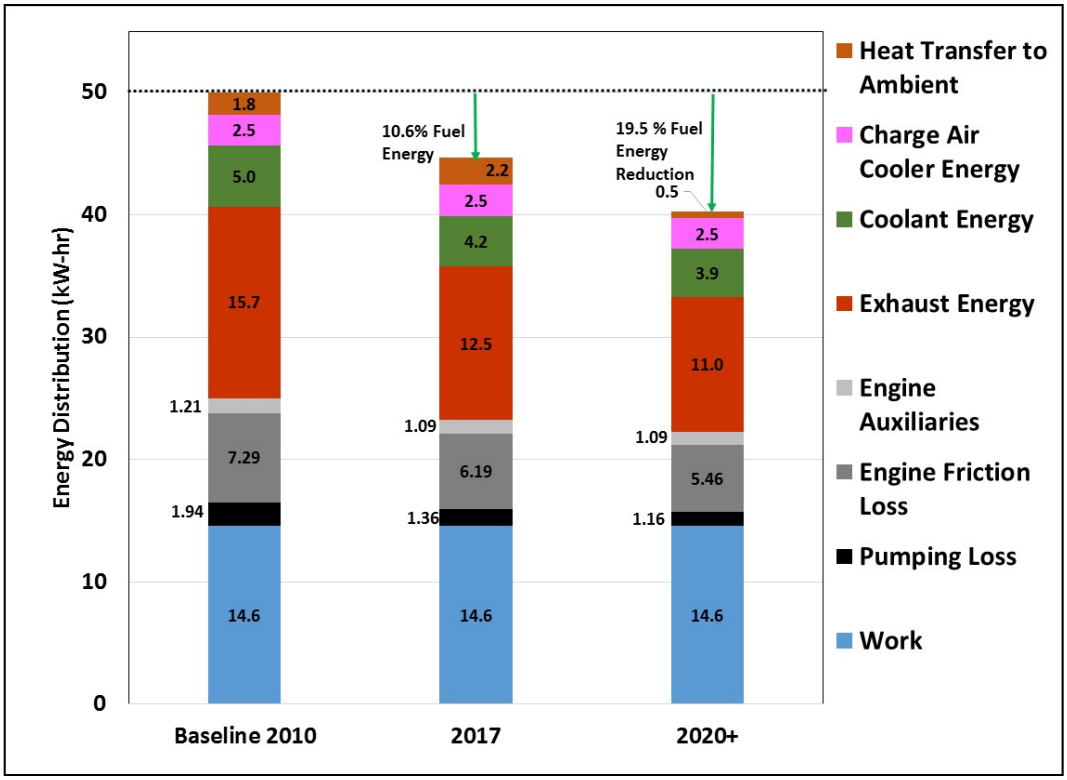

Figure 39 Medium-duty energy loss distribution for 2010, 2017 and 2020+ engine technologies over FTP

5.6 Waste Heat Recovery

Waste heat recovery simulations were performed to extract heat from EGR and coolant circuits. The results below show the total WHR potential under the lug curve of both the heavy-duty and medium-duty diesel engine. There are some feedback loops and control issues between the WHR and engine systems that cannot be captured by a simple steady-state Rankine cycle simulation. In addition, the ORC simulation was performed on the energy distribution measured on the baseline 2010 engines. Since, the energy distribution of future engines could be significantly different from the baseline 2010, conclusions of WHR potential from future engines cannot be drawn easily. The heat available for recovery depends on various engine transient parameters such as engine load, coolant flow, EGR flow rates, temperatures and flow of exhaust stream. Hence the transient prediction of WHR is a challenging task and highly impractical. We assume a simple steady-state map of WHR that does not take into account the aforementioned complexities. The WHR model simulated in this study optimized the working fluid flow to achieve maximum turbine work output.

The results of the WHR model were incorporated into a potential 2020+ technology fuel map by reducing the fuel input in order to match the actual BTE that the reference engine with WHR would produce. The brake work needed to remain constant since its value is constrained by the use of lookup tables (any cell in the table already corresponds to a torque-speed combination). To better illustrate the process, the following example shows the incorporation of WHR at a single operational point of the engine.

Illustrative example:

$$WHR\ work\ output\ =\ 25\ KW$$

$$Speed = 1320\ rpm$$

$$Torque = 757\ N-m$$

$$Brake\ power = 105\ kW$$

$$Reference\ engine\ input\ fuel\ energy = 6.41\ g/sec\ X\ 42.8\ KJ/kg = 274.34\ kW$$

$$Reference\ engine\ BTE = \frac{105}{274.34} = 38.2\%$$

$$New\ BTE\ with\ WHR\ power = \frac{(105+25)}{274.34} = 47.3\%$$

$$New\ input\ fuel\ energy\ to\ Match\ BTE\ for\ baseline\ work = \frac{105}{0.473} = 221.98\ KW$$

$$Percent\ reduction\ in\ fuel\ energy = \frac{274.34-221.98}{274.34} = 19\%$$

Note that the 19% fuel consumption reduction in the example above is a conservative estimate when compared with other studies (Park et al., 2011, Teng et al., 2011) that calculate fuel consumption benefit as the ratio between power recovery and base engine power (25kW/105kW = 23.8% fuel consumption reduction based on example above).

5.6.1 USEPA 2010 Heavy-Duty Diesel Engine WHR Model

Figures 40 and 41 show the total available waste heat from the engine coolant circuit and EGR circuit under the engine lug curve, respectively. Under the high load, operating points of the engine the WHR ORC simulation recovers about 15% of the total available waste heat. The WHR output power obtained from WVU simulations is comparable to the outputs simulated and observed by Cummins WHR design (Nelson, 2008a). Nelson reported a 19.4 hp observed power output at 1600 rpm and 450 bhp engine output.

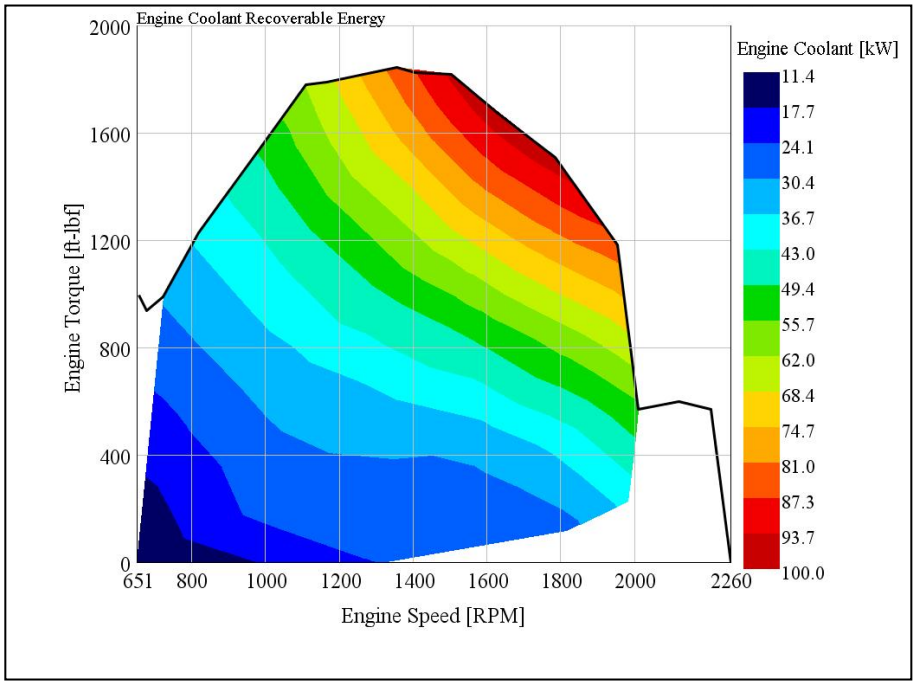

Figure 40. Recoverable energy from engine coolant circuit for USEPA 2010 heavy-duty engine

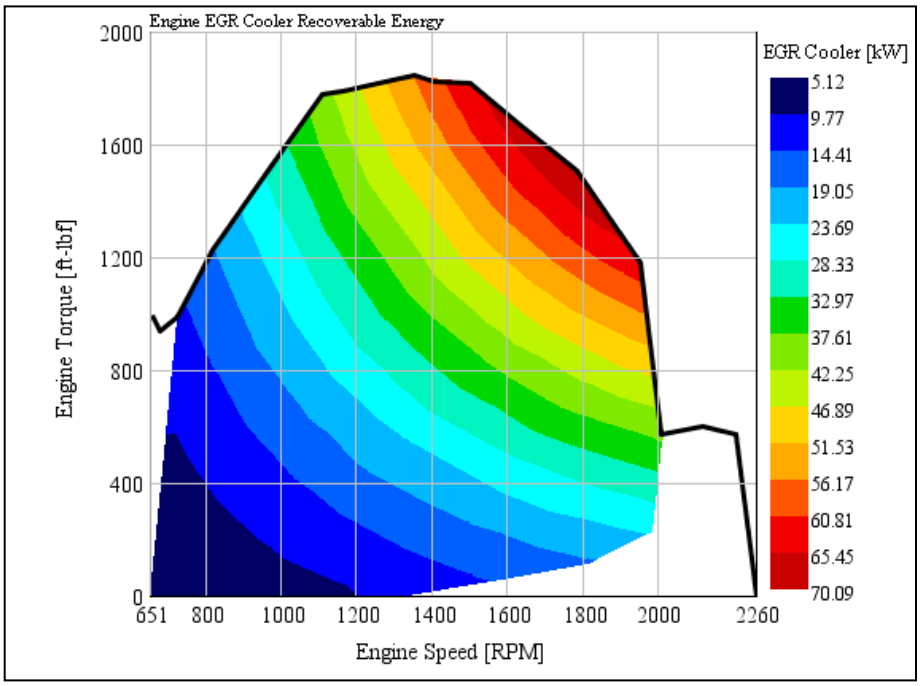

Figure 41. Recoverable energy from EGR cooler for USEPA 2010 heavy-duty engine

Figure 42 shows the contour of WHR output work potential from an ORC simulated on the Mack MP8 heavy-duty diesel engine. The results show that the bulk of the WHR potential is available only during the higher load engine operation that is characterized by higher EGR energy and higher coolant energy. The WHR potential close to the rated engine speed is around 25 kW. While the medium load regions of the lug curve, show a WHR potential close to 16 kW.

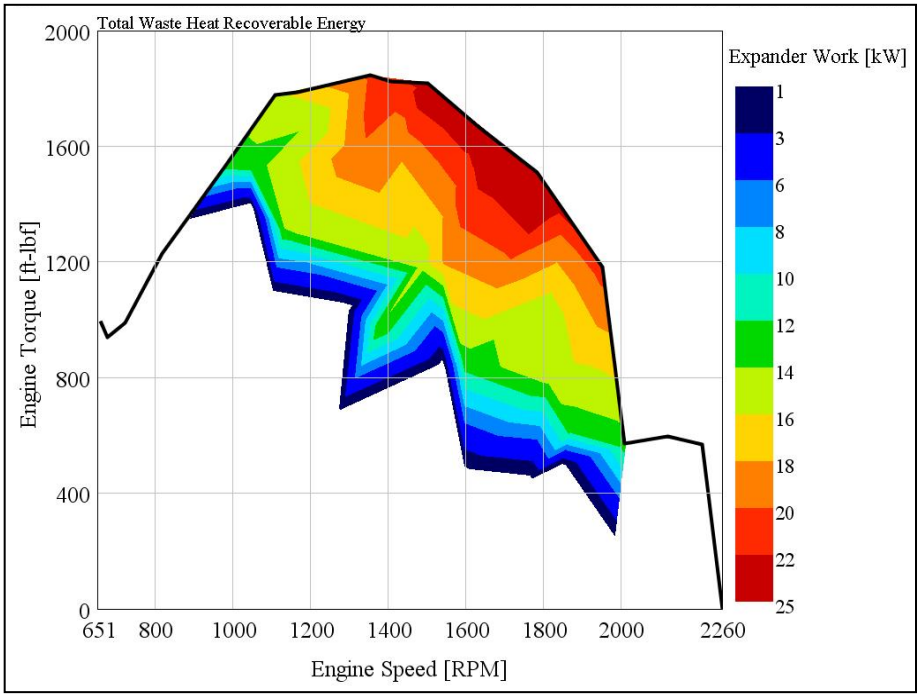

Figure 40. Result for total recoverable turbine output work from WHR model for USEPA 2010 heavy-duty engine

5.6.2 USEPA 2010 Medium Duty Diesel Engine WHR Model

Figures 43 and 44 show the total available waste heat carried by the engine coolant and EGR circuit of the Cummins ISB6.7, respectively. The results showed a maximum of 54 kW of heat is rejected by coolant under the medium-duty engine's lug curve. The EGR circuit of the medium-duty platform showed a maximum of 42 kW available for the waste heat recovery process. Heat energy rejected by EGR in a medium duty engine is significantly lower than the heavy-duty platform. This can be attributed to lower EGR fractions due to better NOx control using SCR activity with close-coupled aftertreatment systems. As a result the available WHR work output is lower than results achieved in the heavy-duty platform.

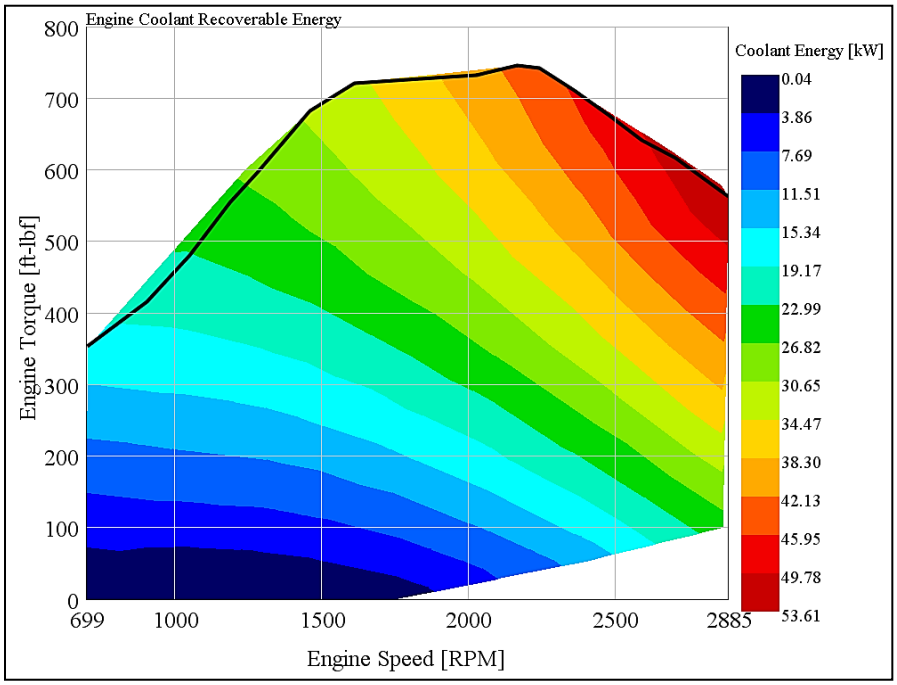

Figure 43. Recoverable energy from engine coolant circuit of medium-duty USEPA 2010 engine

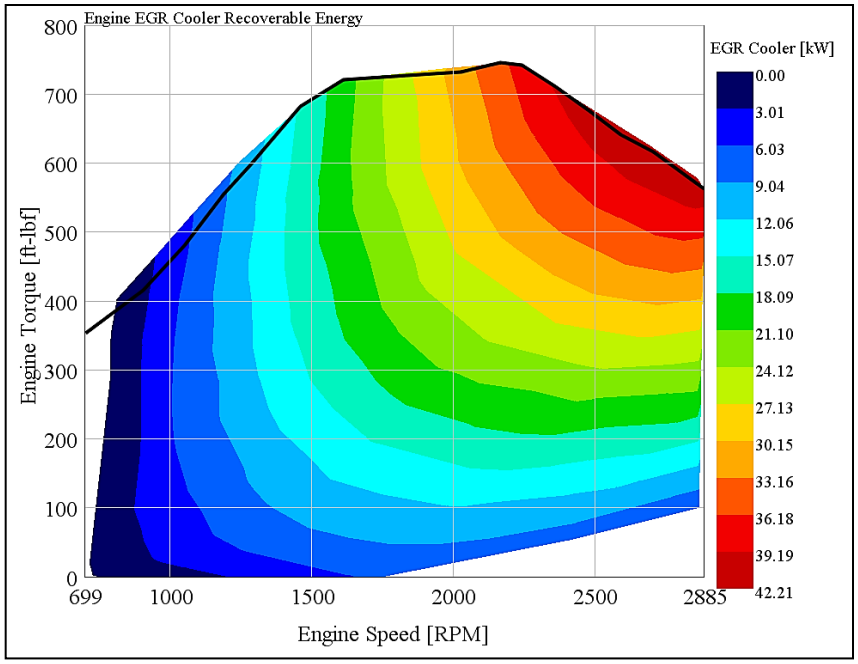

Figure 44. Recoverable energy from EGR circuit for medium-duty USEPA 2010 engine

Figure 45 shows the WHR output work potential simulated on the medium-duty Cummins ISB6.7 engine platform. Maximum WHR potential in the medium-duty platform is realized in the full load regions of the higher engine speed regions. The simulation shows a maximum of 11 KW achievable from ORC WHR simulations. However, medium-duty diesel engines are used in vocational vehicles which tend to operate in transient, relatively low average speed duty cycles, which make the engine to mainly operate in regions outside the region shown in Figure 43. It can be inferred that the WHR potential from medium-duty platform is not significant factor for engine efficiency improvement.

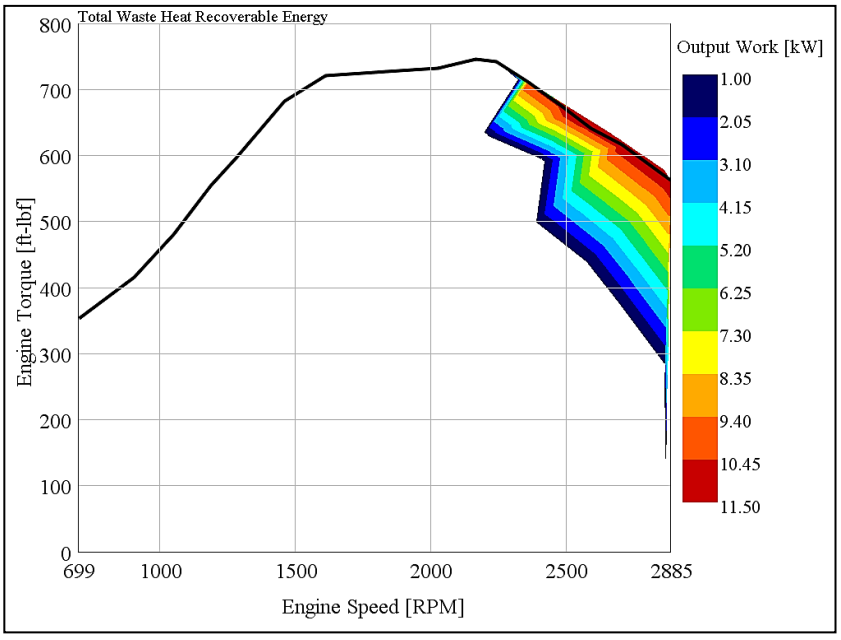

Figure 45. Result for total recoverable turbine output work from WHR model for medium duty USEPA 2010 engine

6 CONCLUSIONS

This work sought to better understand the efficiency, the energy losses, and the prospects for improvement in diesel engines for heavy- and medium-duty vehicles. The project's approach involved laboratory engine testing and analysis of two baseline diesel engines that are compliant with model year 2010 U.S. Environmental Protection Agency emissions standards. The engines tested were a 12.8-liter heavy-duty diesel engine, representative for Class 8 tractor-trailers, and a 6.7-liter medium-duty engine, representative of Class 4-6 trucks (e.g., urban delivery, vocational). Additional engine data were used to further refine and validate efficiency data. In addition, data from industry colleagues and from the research literature were utilized to understand the changes in energy flows and losses from various efficiency technologies.

The two primary outputs from the work were the characterization of the engine maps of modern engines, and detailed energy audit analyses across varying engine load conditions (i.e., over varying torque and speed points) of those engines. The engine fuel maps were developed for the baseline 2010 heavy-duty and medium-duty engines by testing them over a test matrix that included a series of steady-state points with transients in between the load points. The fuel consumption data developed from this procedure was used to populate 25 x 25 fuel matrix using a 2^{nd} order surface fit of the data. The energy audits over 50 steady-state points were conducted to characterize the distribution of input energy as engine losses and useful work.

The reference heavy-duty diesel engine converted 39.1% of its fuel energy to brake power over the SET engine cycle, with 35.5% lost as exhaust heat, 10.6% lost to engine coolant heat transfer, 6% lost through heat rejected from the charge air cooler (CAC), 3.4% lost as heat to the surrounding ambient air, 2.3% lost to friction of engine components, 1.7% lost to engine pumping, and 1.3% consumed by parasitic losses due to engine accessories such as water and oil pumps. The contribution of EGR cooling to the engine coolant circuit is of the order of 46% of the total heat carried by the coolant. While the reference medium-duty diesel engine over the FTP cycle converted 29.2% of its fuel energy to brake power, 31.4% of fuel energy was lost through exhaust gases, 18.4% of energy loss is attributed to friction and pumping loss, 10% of fuel energy was rejected through the coolant circuit, CAC rejected 5% of fuel energy, 3.6% of fuel energy is attributed to heat transfer to ambient air, and 2.4% of fuel energy was consumed by engine accessories.

The study further used the energy audit and technology forecasting to investigate emerging technologies' ability to reduce fuel consumption by targeting each of the loss mechanisms. Two potential future engines were analyzed: (1) a "2017 engine" for heavy-duty vehicle engine standards, and (2) a "2020+ diesel engine" that utilizes more advanced technologies for further fuel consumption reduction. The investigation of emerging technologies to achieve the improved efficiency included increased compression ratio, optimized controls, exhaust gas recirculation improvements, low-friction lubricants, engine friction reduction, parasitic load reduction (piston, water pump, oil pump, fuel pump), turbocharging improvements, fuel injection, optimized cylinder head design, and waste heat recovery systems.

The analysis indicated that these emerging engine efficiency technologies have the ability to substantially reduce fuel consumption. The estimated 2017 engine cycle achieved an average 7.9% fuel consumption reduction over the SET engine cycle, while the more advanced 2020+ engine achieved an average 18.3% fuel consumption reduction over the SET cycle in comparison to the baseline 2010 heavy-duty engine. For the prediction of the 2017 engine, the study considered reduced engine friction, improved turbomachinery, improved efficiency of engine accessories, and reduced pumping loses due to lower

aftertreatment and EGR loop backpressure. In addition to these technologies, a WHR simulation was performed to incorporate in to the engine efficiency improvement pathway to predict 2020+ fuel consumption. The peak BTE of the 2020+ engine was projected to be 49%, and the waste heat recovery simulation improved the BTE of the 2020+ engine to 52%. Technology improvements such as turbo compounding, engine down speeding and integrated engine and transmissions show promise towards achieving a 55% BTE target. This study restricted its analysis to thermodynamic loss mechanisms in the engine and its subsequent impact on fuel consumption.

The study also performed a simple WHR based on the ORC design using R245fa as the working fluid. The work output of the turbine was incorporated into the 2020+ engine prediction to reduce the input fuel energy. The WHR simulation on the heavy-duty platform showed peak WHR power output of 25 kW while the medium-duty showed a peak WHR output power of 12 kW. The medium duty platform does not show a significant WHR potential over its main operational region due to lower EGR fractions and less coolant heat rejection. A combination of effective SCR operation and lower coolant heat rejection lowers the available energy for WHR system.

The prediction methodology in this research work did not assume any cross effects between factors. For example, higher injection pressures will also affect fuel pump work, and efficient engines will result in lower exhaust heat resulting in lower WHR potential. Since the study considered only the positive impacts without the potential negative cross-effects of a certain engine technology or efficiency improvement pathway, the results presented in this study could be different from real-world engine efficiencies that could be achieved with future engine technologies. Further, the study also assumes a fuel consumption reduction throughout the lug curve, while in a practical case, it can be expected that the engines would be calibrated to operate in a narrow speed range with highest efficiency. Since, the prediction of integrated engine and transmission with associated speed and load based efficiency gain is beyond the scope of the study, this study presents a holistic approach on fuel consumption reduction through a basic thermodynamic analysis that focuses on the main energy loss categories in an engine. It is also important to note that diesel engine efficiency is constantly constrained by the need to meet stringent emissions and durability, and therefore the impact of engine efficiency gains on exhaust aftertreatment activity is an interesting research direction that has broad implications towards future emissions compliance procedures. The utilization of WHR technology for thermal management strategies could possibly alleviate the issues related to aftertreatment activity related to lower available exhaust energy.

This research makes novel contributions in providing a detailed breakdown of engine energy loads and losses for a modern heavy- and medium-duty diesel engine over a large region under the lug curve. This research work also estimated potential fuel consumption improvements from future technology improvements in the heavy-duty diesel engines. The research points towards many directions where future research will better inform the potential for heavy-duty diesel efficiency improvements. For example, integrating work like this with full-vehicle simulation will be critical to fully understand engine-transmission and powertrain-vehicle load interactions with emerging efficiency technologies for the 2020-2030 timeframe. In addition, the energy savings are not uniformly distributed over all engine operation load points; variations for different engines size and vehicle duty cycles could result in substantially different real-world results.

7 REFERENCES

ARDANESE, R. 2008. Control of NOx and PM emissions from SCR-equipped 2010 compliant Heavy-Duty Diesel Engine over Different Engine-Out Calibrations. Doctor of Philosophy, West Virginia University.

CALLLAHAN, T., BRANYON, D., FORSTER, A., ROSS, M. & SIMPSON, D. 2012. Effectiveness of Mechanical Turbo Compounding in a Modern Heavy-Duty Diesel Engine. International Journal of Automotive Engineering, 3, 69-73.

CHEBLI, E., MULLER, M., LEWEUX, J. & GORBACH, A. 2013. Development of an Exhaust-Gas Turbocharger for HD Daimler CV Engines. MTZ Worldwide, 74, 24-29.

CONCENTRIC. 2014. http://www.concentricab.com/Engines2.asp?cat=3&subcat=32&subsubcat=321 [Online]. [Accessed 4/30/2014].

COOPER, C., KAMAKATE, F., REINHART, T., KROMER, M. & WILSON, R. 2009. Reducing Heavy-duty Long Haul Combination Truck Fuel Consumption and CO2 Emissions. In: MILLER, P. (ed.).

CORNING Corning DuraTrap AC Filters. In: INC., C. (ed.) http://www.corning.com/environmentaltechnologies/products_services/particulate_filters.aspx.

CUMMINS. 2014a. New Technologies Revealed at IAA Hannover Ignites Fuel Efficiency Debate [Online]. Cummins Turbo Technologies. [Accessed 7/15/2014 2014].

CUMMINS. 2014b. Secrets of Better Fuel Economy- The physics of MPG [Online]. Available: http://cumminsengines.com/uploads/docs/cummins_secrets_of_better_fuel_economy.pdf [Accessed 7/31/2014].

DAIMLER 2014. http://www.demanddetroit.com/engines/DD15/ [Online]. [Accessed 4/30/2014].

DELGADO, O. & LUTSEY, N. 2014. The U.S. SuperTruck Program – Expediting the development of advanced heavy-duty vehicle efficiency technologies. International Council for Clean Transportation.

FENSKE, G. R., ERCK, R. A., AJAYI, O. O., MASONER, A. & COMFORT, A. S. 2014. Impact of friction reduction technologies on fuel economy for ground vehicles. US Army RDECOM-TARDEC.

GRANT, S. 2004. Piston ring design for reduced friction in modern internal combustion engines. Master's Degree, Massachusetts Institute of Technology.

GRESZLER, T. Year. Volvo's Achievements and Plans for Fuel Efficiency and GHG Reduction. The Role of the Internal Combustion Engine in our Energy Future. In: Diesel Engine-Efficiency and Emissions Research (DEER) Conference, 2011 Detroit, Michigan. DOE.

HANSON, C., HELTON, J. C. & SALLABERRY, C. J. 2012. Use of replictaed latin hypercube sampling to estimate sapling variance in uncertainity and sensitivity analysis results for the geological disposal of radioactive waste. Reliability engineering and system safety, 107, 139-148.

IMAN, R. L., DAVENPORT, J. M. & ZEIGLER, D. K. 1980. Latin Hypercube sampling (A Progran Users Guide). Albuquerque: Sandia National Laboratories.

LASECKI, M. & COUSINEAU, J. 2003. Controllable Electric Oil Pumps in Heavy Duty Diesel Engines. SAE, SAE-2003-01-3421.

MAGO, P. J., CHAMRA, L. M. & SOMAYAJI, C. 2006. Performance analysis of different working fluids for use in organic Rankine cycles. Proceedings of Instituion of Mechanical Engineers, Part A Journal of Power and Energy, 221, 255-264.

MCKAY, M. D., BECKMAN, R. J. & CONOVER, W. J. 1979. A Comparison of three methods for selecting values of input variables in the analysis of output from a computer code. Technometrics, 21, 239-245.

NELSON, C. 2008a. Exhaust Energy Recovery- 2008 DEER Conference.

NELSON, C. 2008b. Waste Heat Recovery for Heavy-duty Vehicles [Online]. Available: http://www.steampower.com/publications/Cummins2008.pdf [Accessed].

NRC 2010. Technologies and Approaches to Reducing the Fuel Consumption of Medium- and Heavy-Duty Vehicles. In: PRESS, T. N. A. (ed.). Washington D.C.

NRC 2014. Reducing the Fuel Consumption and Greenhouse Gas Emissions of Medium- and Heavy-Duty Vehicles, Phase Two: First Report. Committee on Assessment of Technologies and Approaches for Reducing the Fuel Consumption of Medium- and Heavy-Duty Vehicles, Phase Two; Board on Energy and Environmental Systems. In: DIVISIONS OF ENGINEERING AND PHYSICAL SCIENCES, T. R. B. (ed.). National Research Council.

PACKHAM, N. & SCHMIDT, W. M. 2008. Latin hypercube sampling with dependence and applications in finance. Frankfurt School of Finance and Management, Centre for Practical Quantitative Finance (CPQF).

PARK, T., HO, T., HUNTER, G., VELDE, B. & KLAVER, J. 2011. A Rankine Cycle System for Recovering Waste Heat from HD Diesel Engines - Experimental Results. SAE, SAE 2011-01-1337.

ROBERTS, C., STOVELL, C., ROTHBAUER, R. & MEHTA, D. 2011. Advancements in Diesel Combustion System Design to Improve Smoke-BSFC Tradeoff. International Jouranl of Automotive Engineering, 2, 55-60.

SACKS, J., WELCH, W. J., MITCHELL, T. J. & WYNN, H. P. 1989. Design and analysis of computer experiments. Statistical Science Statistical Sciences, 4, 409-423.

STANTON, D. 2009. Technology Development for High Efficiency Clean Diesel Engines and a Pathway to 50% Thermal Efficiency.

STANTON, D. 2013. Systematic Development of Highly Efficient and Clean Engines to Meet Future Commercial Vehicle Greenhouse Gas Regulations. SAE, 2013-01-2421.

TAN, J., SOLBRIG, C. & SCHMIEG, S. 2011. The Development of Advanced 2-Way SCR/DPF Systems to Meet Future Heavy-Duty Diesel Emissions. SAE International, 2011-01-1140.

TENG, H., KLAVER, J., PARK, T., HUNTER, G. & VELDE, B. 2011. A Rankine Cycle System for Recovering Waste Heat from HD Diesel Engines - WHR System Development. SAE, 2011-04-12.

USEPA 2014. Engine Certification Data [Online]. Available: http://www.epa.gov/otaq/certdata.htm [Accessed 7/14/2014].

USEPA 2011. Final Rulemaking to Establish Greenhouse Gas Emissions Standards and Fuel Efficiency Standards for Medium- and Heavy-Duty Engines and Vehicles.

WHITE HOUSE 2014. Remarks by the President on Fuel Efficiency Standards of Medium and Heavy-Duty Vehicles. http://www.whitehouse.gov/the-press-office/2014/02/18/remarks-president-fuel-efficiency-standards-medium-and-heavy-duty-vehicl

8 APPENDIX

a) **Latin Hypercube design**: Latin hypercube sampling is a form of stratified sampling described by McKay (Mckay et al., 1979) and elaborated upon by Iman et al., (Iman et al., 1980) that can be applied to multiple variables. Variables are sampled using an even sampling method, and then randomly combined sets of those variables are used for one calculation of the target function. A sampling algorithm ensures that the distribution function is sampled evenly, but still with the same probability trend. To perform the stratified sampling, the cumulative probability (100%) is divided into segments. A probability is randomly picked within each segment using a uniform distribution, and then mapped to the correct representative value in of the variable's actual distribution. Latin hypercube sampling has distinct advantages, primarily ease of computation. Typically one third as many Latin hypercube iterations are required to as equivalent Monte Carlo iterations. Disadvantages include highly skewed distributions require more iterations, and the simulation must be run until completion, i.e. interrupted or incomplete results are inaccurate. Latin hypercube sampling is frequently a standard technique in statistical packages, and has been widely utilized in a variety of fields, for example from financial risk analysis (Packham and Schmidt, 2008) to radioactive waste disposal uncertainty (Hanson et al., 2012). This methodology considers two factors (speed and torque) consisting of multiple levels. Multiple levels of speed are bounded on the lower end by idle and on the upper end by the high idle (governed speed of the engine). The torque levels at each speed are bounded on the lower end by 0% of peak torque at that speed and the upper end by 100% torque at current speed. The points are then chosen to maximize the minimum distance between design points while maintaining the spacing between factor levels constant.

b) **Gaussian Process IMSE Optimal design**: The Gaussian IMSE process was first proposed by Sacks et al., (Sacks et al., 1989) minimizes the integrated mean squared error of the Gaussian process model over the design region. Gaussian IMSE models are widely used in computer simulation research. When used in physical experiments, Gaussian IMSE models use an objective criterion to fill in a design space. This design methodology originally created to capture complex behavior between one or more predictors tries to minimize the integrated mean squared error of the selected points. In addition to the set points identified by the DOE approach, additional points were selected to better characterize the high load points under the lug curve. In specific three 100% load points from the European Stationary Cycle (ESC). This ensured that the full load operation was also captured.

Table A1 FTP emissions results for the heavy-duty Mack MP8

	2012- Mack MP8		
	FTP1	**FTP2**	**FTP3**
CO2 (g/bhp-hr)	522.7	522.1	522.1
CO (g/bhp-hr)	0.714	0.791	0.750
NOx (g/bhp-hr)	0.136	0.154	0.136
NO (g/bhp-hr)	0.124	0.132	0.113
Fuel consumption (kg)	5.9	5.9	5.9
Brake Work (bhp-hr)	36.7	36.8	36.7

Table A2 SET emissions results for the heavy-duty Mack MP8

Speed (rpm)	**Torque (ft-lbs)**	**Fuel Consumption (g/sec)**	**Instantaneous CO2 (g/sec)**	**Work (bhp-hr)**	**Brake specific-CO2 (g/bhp-hr)**
650	0	0.5	-	-	-
1206	1719	17.3	53.7	13.2	489.8
1460	891	10.7	33.1	8.3	481.1
1460	1343	15.9	49.22	12.4	474.6
1206	884	8.7	26.99	6.8	478.7
1206	1322	12.9	39.78	10.1	471.8
1206	440	4.8	14.73	3.4	524.8
1460	1806	21.7	67.6	16.7	484.7
1460	449	5.9	18.55	4.2	535.0
1715	1581	22.2	71.56	17.2	499.0
1715	391	6.6	20.18	4.3	569.0
1715	1174	16.8	52.25	12.8	490.7
1715	782	11.5	35.41	8.5	499.2
				Composite	492.2

Table A3 FTP emissions results for the medium-duty Cummins ISB6.7

	2011- Cummins ISB6.7		
	FTP1	**FTP2**	**FTP3**
CO2 (g/bhp-hr)	632.4	633.9	634.4
CO (g/bhp-hr)	0.086	0.087	0.079
NOx (g/bhp-hr)	0.31	0.31	0.31
NO (g/bhp-hr)	0.286	0.303	0.299
Fuel consumption (kg)	4.00	4.01	4.02
Brake Work (bhp-hr)	20.51	20.52	20.52